University of Groningen
Bachelor Project

Geometry and microstructure of multilayer laser cladded coatings

Student: Natascha Koelewijn (s1771639)

Supervisors: prof dr. J.Th.M. De Hosson, dr. V. Ocelík, ing. O. Nenadl

Table of Contents

1 Introduction

1.1 Laser cladding

Laser cladding has become the process of choice in many applications involving coating, repair and reworking. It is a process particularly suitable for the production of small, discrete surface clads with arbitrary thickness (0.05-2.5mm) and track width (0.4-15 mm) [1][2].

It offers many advantages over conventional coating processes as this technique can produce a much better coating, with less dilution, minimal distortion, and better surface quality. The benefits of using laser cladding technology due to its additive nature are: reduction of production time, enhancement of thermal control, parts and coating repair, production of a functionally graded part, and a smart structure by encapsulation [1].

During laser cladding of a clad metal onto a metal substrate a chemical bonding occurs between the substrate and coating areas. This type of chemical bonding is referred to as metallurgical bonding. It is free from oxide films, voids and any forms of discontinuities [1].

1.1.1 Basic principle

The basic principle of laser cladding is to use a high power laser beam that scans and melts the surface locally while additional material is added in the form of preplaced wire feeding or simultaneously via coaxial or side feeding of powder particles to create a melt pool, which solidifies on the surface forming the coating [1][3]. In this research the latter two are used.

The coaxial nozzle has a circular feeding around the laser beam and the side nozzle adds the powder from the side of the laser beam. For both nozzles the powder is being fed using a carrier gas, while a shielding gas shields the laser beam as well as preventing oxidation. Often argon and nitrogen are being used for this application [2]. A schematic overview of the laser cladding process can be found in Fig. 1.

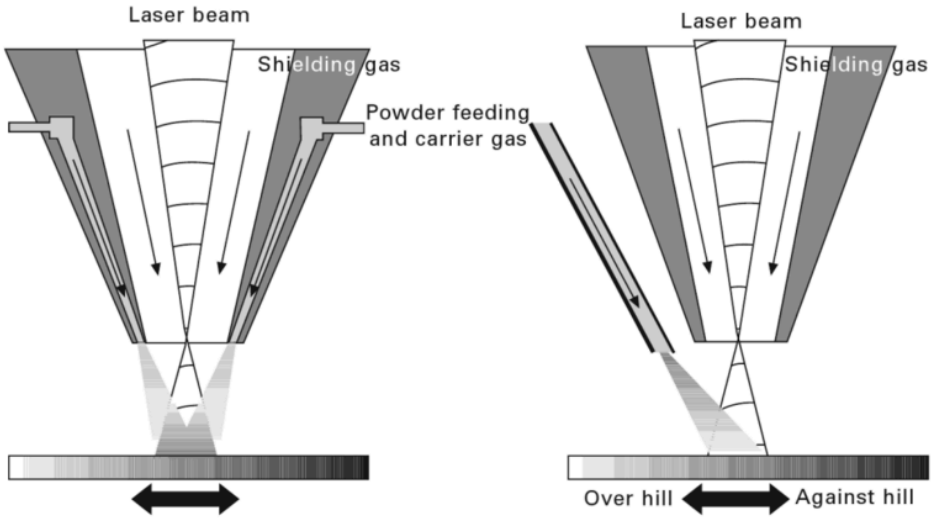

Fig. 1. Schematic view of a coaxial (left) and side (right) laser cladding set-up above a moving substrate [4].

There are two cladding conditions relevant for side cladding to deliver the powder stream with respect to the laser beam. These conditions are so-called “against hill” where the powder is applied from the side where the substrate moves, and “over hill” where the powder is fed from the opposite side. [4]

When the powder stream is delivered coaxially with the laser beam, all directions of the substrate movement perpendicular to the laser beam are equivalent. The coaxial process is therefore independent of the cladding direction. This makes it possible to produce equivalent tracks independent of the substrate movement direction. [4]

1.1.2 Laser processing parameters

In laser cladding there are several parameters which can be controlled and influence the properties of the clad. One of the main components of the laser cladding process is the laser beam itself. The laser beam is usually defocused on the clad surface to give a larger clad area. The amount of defocus can be changed, which allows for selection of a desired coating width. Also the laser beam is tilted over a small angle to avoid back reflecting.

The main parameter from the laser is the laser power P [W]. Insufficient power will result in limited melting of the powder, whereas too much power causes melting of the substrate and dilution of the clad. [5]

To clad over a certain area the substrate moves with a certain speed with respect to the laser beam, this speed can be controlled and is referred to as scanning speed S [mm/s] [5]. The scanning speed is of considerable importance to the shape of its solidification front, i.e. the fibre texture orientation and grain orientation [3]. For overlap of tracks, low scanning speeds give sharp microstructural discontinuities [3].

Besides choosing a different type of nozzle or a nozzle with a different size the amount of powder fed can be adjusted and is called powder feeding rate F [mg/s]. If the rate is too low, the excessive heat of the laser will cause the substrate to melt. On the other hand, if it is too high the powder shields the substrate from the beam and the coating is more likely to detach from the substrate [2]. The amount and type of shield and carrier gas for the powder feeding can be controlled but do not influence the clad process significantly [2].

It has been experimentally shown that the height of the clad, H, depends linearly on the combined parameter F/S, which is the amount of powder provided per unit length of the laser track, whereas the laser power P has minimal effect on the height of the clad. In a similar way, the width, w, linearly depends on $P/\sqrt{S}$ and the clad area A_C (defined in Fig. 3), which is controlled by the parameter $\sqrt{P}*F/S$ [6]. Fig. 2 shows the dependence of the laser track width and height on the combined laser parameters for the specific set-up used in this research.

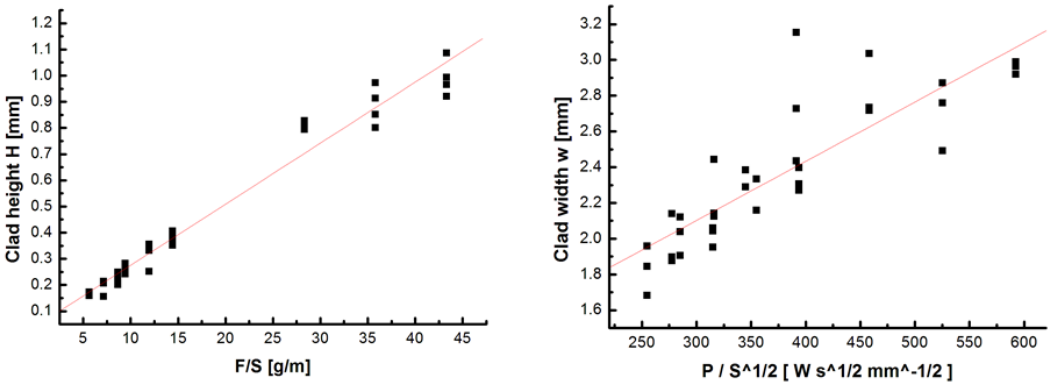

Fig. 2. Empirical dependence of laser track height and width on combined processing parameters observed from coaxial cladding setup for Höganäs 3533-00 powder on SS304 substrate, fitted with straight lines. [8]

1.2 Geometrical model

1.2.1 Main dimensions

After cladding, a transverse cut of a typical single clad on the substrate looks like Fig. 3. Such a clad is described by the height H [mm] and width w [mm] of the track. The height and width are the first important parameters used when modelling a cladded coating. Cladding parameters, e.g. the scanning speed, the powder feeding rate and the laser power, influence these dimensions as discussed in the previous section.

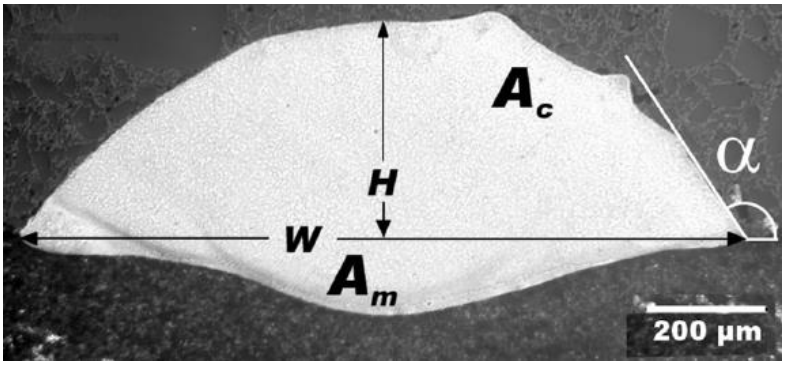

Fig. 3. Cross-sectional view of a single track with dimensions indicated [5].

To clad a complete coating, several clad tracks are deposited next to each other with a certain distance between them. This distance is established during the laser cladding by moving the substrate rod a distance further along the length of the rod after every full rotation. How much this shift is in comparison with the width of one track is defined as the overlap ratio as shown in Fig. 4.

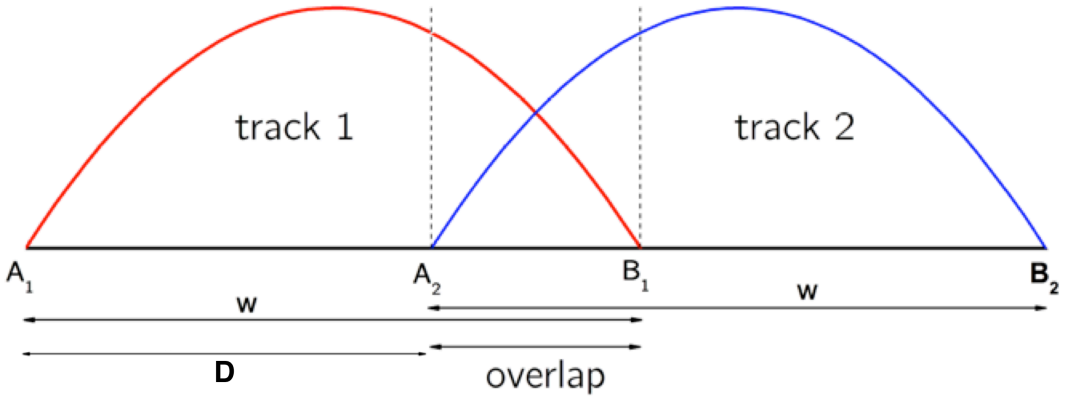

Fig. 4. Definition of two overlapping tracks [5].

As seen in Fig. 4 the distance between starting point of the second track A_2 and the end point of the first track B_1 is the overlap and the overlap ratio (OR) as a percentage ($OR_{\%}$) of the width is defined as follows [8]:

$$OR_{\%} = \frac{w - D}{w} \times 100\%$$

Where w is the width of the individual tracks and D is the distance between the centres of two neighbouring tracks.

By changing the overlap ratio the height and waviness of the coating can be influenced. After a surface is cladded it often needs to be machined to remove remaining waviness. This can result in a less high surface due to more removal of the clad. Too little overlap can result in such a wavy surface or a coating that is too thin. However, too much overlap reduces the coverage rate and may cause a pileup of tracks. [5]

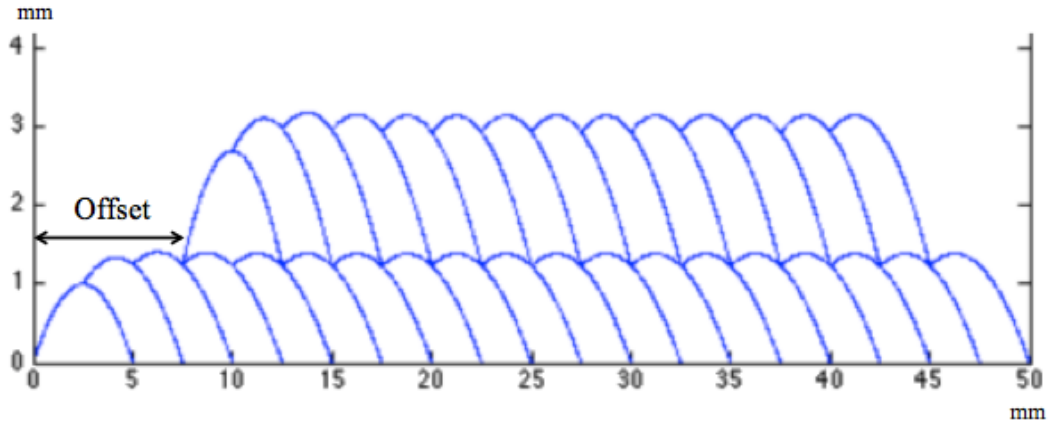

Fig. 5. Offset for multilayer cladded coatings.

For multilayer coatings it is important to have knowledge about the starting point of the consecutive layers relative to the previous layers. This dimension is known as the offset and indicated in Fig. 5. It is the value that indicates where a consecutive layer starts, relative to the previous layer. It is indicated as a percentage of the width of the single track, where A(1,2) is the point A_1 (as used for the first layer in Fig. 4) of the second layer, as follows [7]:

$$OS_{\%} = \frac{A(1,2)}{w} \times 100\%$$

1.2.2 Basic principles

The model works in a recursive way, this means that the shape of each track is calculated with the use of the shape of the previous track via applying the model assumptions. Therefore it is necessary to define and calculate the first track. After this step the next clad layer can be predicted with the same shape as the first (in further steps the previous) track and with the same amount of material cladded. This process can be repeated until a desired amount of tracks is cladded. In previous research it has been shown that parabolic functions describe the geometry of side and coaxial laser cladded coatings best. [5]

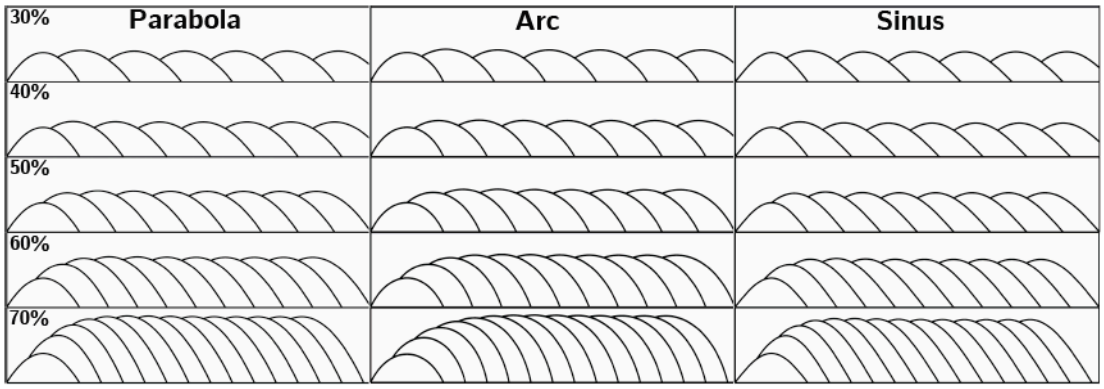

Fig. 6. Purely geometrical output of the overlap model for three different shape functions and five different overlap ratios [5].

1.2.3 Overlap model

The relative coating height and the relative surface waviness depend on the overlap ratio and the shape function. For the design of the model three basic assumptions are made [5]:

1. The width of the track is controlled by the width of the laser beam and stays constant.
2. The track profile shape is not changed by overlap.
3. The amount of material cladded stays constant for each successive track cladded.

Based on the first assumption, the width of the track remains constant and can be controlled by the heat source, for instance by changing the focus of the beam.

The second assumption states that a consecutive track will obey the same shape as the first track. Meaning if we model a layer with the parabolic function, consecutive tracks will also be a parabolic function, with in the case of overlap, different parabolic constants.

The third assumption states that the amount of material that is added to the layer will remain constant. This would be true if all clads would be performed under identical conditions. In the case of overlap, this is not the case since the first track is put on a flat substrate and a consecutive track is cladded on a partially inclined surface (from the previous track). As well as the fact that the tracks for a consecutive layer will not be put on the flat substrate, but on the wavy coating from the previous track [7].

The mathematical form of a parabolic function is:

$$F_i(x) = a_i x^2 + b_i x + c_i \quad F_i(x) = 0; x \notin (A_i, B_i)$$

The parameters of the first track $a_1, b_1,$ and c_1 for the parabolic function can be calculated from the values H and w given at the input [5]. Now that the shape and the parameters of the first track are known, the successive track can be calculated by functions that satisfy the above mentioned assumptions.

$$F_i(A_i) = F_{i-1}(A_i) \quad for \quad i = 2,3, \dots n$$

States that the next track will start on the previous track.

$$F_i(B_i) = 0 \quad for \quad i = 1,2, \dots n$$

This states that the function will become 0 at the end of the track.

$$\int_{A_i}^{B_i} F_i(x)dx = \int_{A_i}^{B_{i-1}} F_{i-1}(x)dx + \int_{A_1}^{B_1} F_1(x)dx$$

The equation above states that the area underneath the next function is equal to the area of the single track plus the area of the previous function, which is also underneath the next. This ensures that each succeeding track adds an equal amount

of "area" (which resembles the clad material) as the first function. By solving these three functions for each succeeding track the three (unknown) parameters can be calculated. And the succeeding coating shapes can be plotted as shown in Fig. 7. [5]

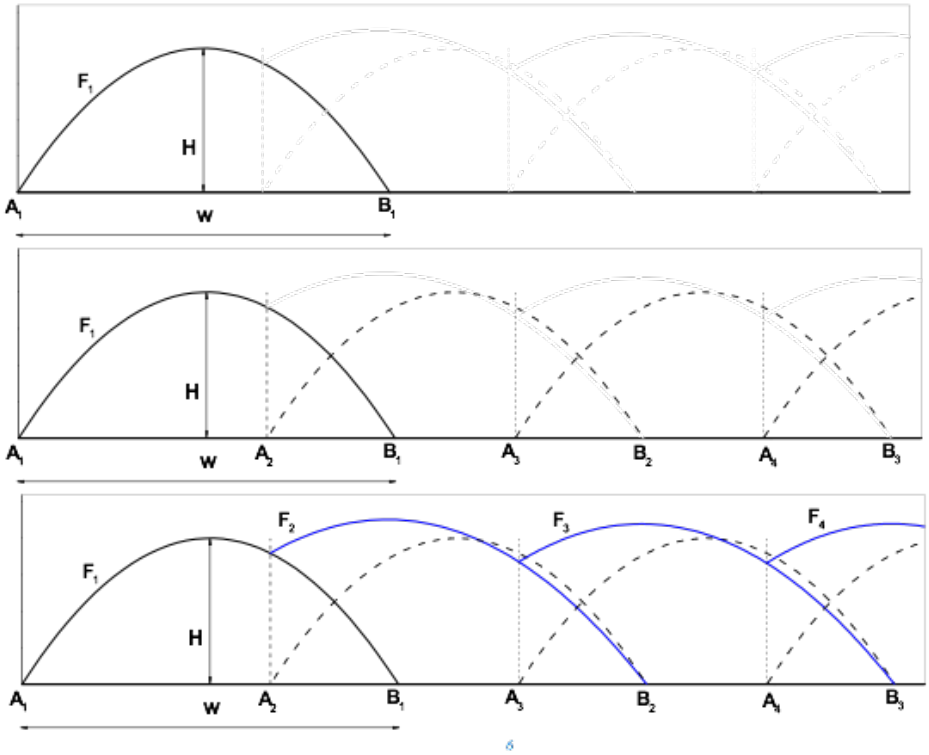

Fig. 7. Illustration of recursive parabolic model overlapping clads to form a single layer [8].

1.2.3.1 Multilayer modifications

For multilayer coatings, the first track of the next layer can span multiple tracks of the previous layer and with an arbitrary chosen offset percentage it could span from track *I* up to *n* [7]. This has been described in previous research to lead to changes in the boundary conditions of the recursive equations. These modifications further complicated the model and a discretization of the x-space in steps of *h* was introduced that has lead to the implementation of a numerical integration by the rectangle method for the calculation of the area of the previous layer. [7]

$$A_{prevlayer} = \sum_{n=k}^{k+N} y(n,j) \times h$$

Where *n* is the index of element in the array where the layer geometry is being stored, *j* the layer number, *N* the amount of steps it takes to numerically integrate the interval from $A_{1,j}$ to $B_{1,j}$, and *k* the index of the element corresponding to $x = A_{1,j}$. [7]

Now, for calculation of a layer all the begin- and endpoints of the tracks are calculated, based on the range that is wanted (width of the coating), width of the track, offset for consecutive layers, overlap, and total amount of layers [7].

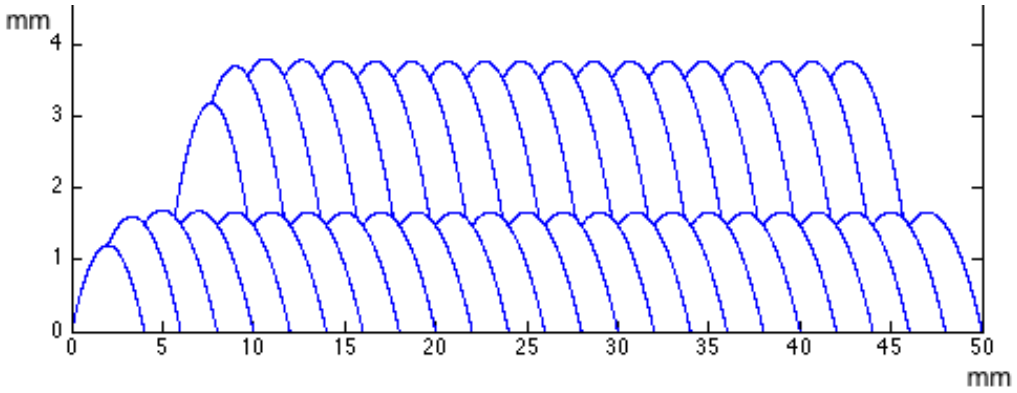

Fig. 8. Example of model output for a double layer clad [7].

1.2.4 Laser parameter model

The laser parameter model takes the combined laser parameters as input for calculation of the width and height of the tracks for the coating. From the plots in Fig. 2 the values (Table 1) for the experimental constants $(\alpha, \gamma, \delta, \omega)$ have been derived for the following equations from the relations shown in the plots: [6]

$$H = \alpha \frac{F}{S} + \gamma$$

$$w = \delta \frac{P}{\sqrt{S}} + \omega$$

Where the values of α, γ, δ and ω are experimental constants that depend on the specific laser cladding set-up. For the set-up used in this research (side feeding with Höganäs 3533-00 powder on SS304 substrate) they have been determined to be:

Table 1. Experimental constants for a set-up with Höganäs 3533-00 powder cladded on SS304 substrate using a side nozzle.

α [mm^2/mg]	γ [mm]	δ [$mm^{1/2} W^{-1} s^{-1/2}$]	ω [mm]
0.02334	0.04207	0.00331	1.10778

The experimental constants depend on the particular set-up, but these can be determined experimentally leading to a prediction of the final laser clad geometry [6]. The constants from Table 1 are obtained in clad experiments where a similar set-up was used as in this research. When any of the following change: cladding type, powder, or substrate the values need to be obtained for the new experimental constants.

1.3 Microstructure

The high rate of cooling during solidification is an important characteristic of laser deposition technologies. It is believed to improve the functional properties of the deposits such as hardness, strength and wear resistance [5]. These improvements are due to microstructural changes due to the cladding process. Typically Electron Backscatter Diffraction (EBSD) is used to explore such microstructures, revealing texture, defects, grain morphology and deformation.

1.3.1 EBSD

EBSD is a microstructural-crystallographic characterisation technique to study any crystalline or polycrystalline material. It works by placing a well-polished sample under an angle in an electron microscope.

For an ordered structure, the atomic planes diffract electrons. The resulting Kikuchi patterns are indexed using a reference structure (here: austenite) and determine the orientation of the crystal from the diffraction pattern after impinging a phosphor screen, thus creating visible lines which are then captured by a CCD camera. A schematic overview of how these Kikuchi patterns (Fig. 10) are determined from the incident electron beam can be found in Fig. 9.

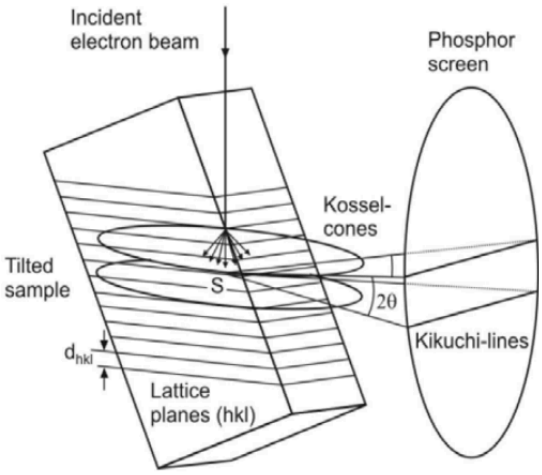

Fig. 9. Schematic overview Kikuchi patterns production [9].

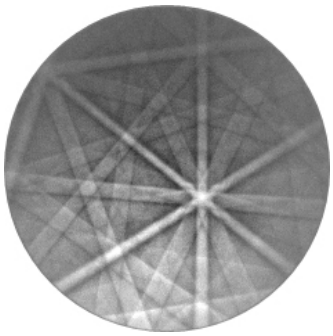

Fig. 10. Example of an austenite Kikuchi pattern [10].

1.3.2 Microstructural characteristics

The left part of Fig. 11 is a sketch of the melt pool and solidification front shape in the longitudinal cross-section in the centre of the laser track. Vector U represents the velocity of the solidification front as a whole for the steady-state cladding process, while U_s and U_t are the normal and tangential components of the local shape of the solidification front curve.

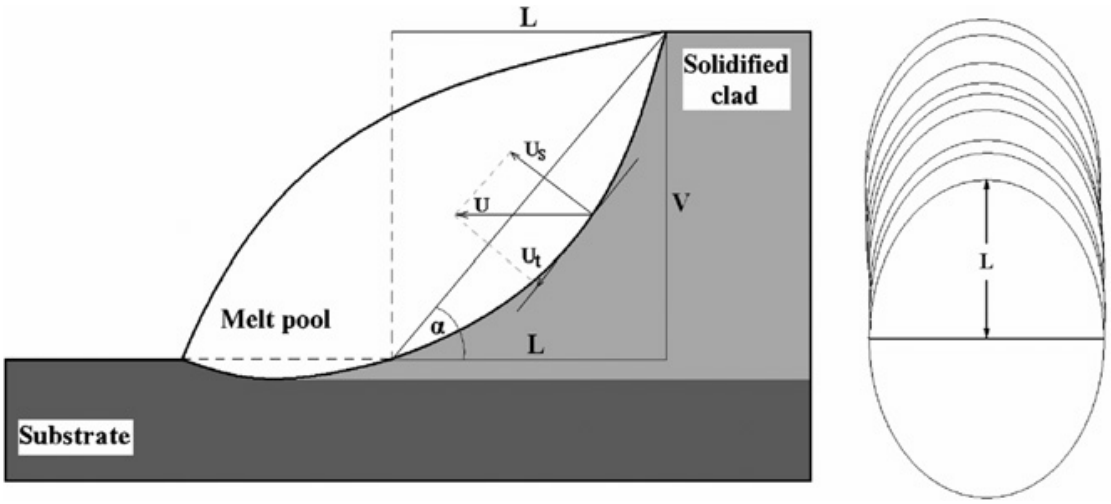

Fig. 11. A sketch of the shape of the melt pool and solidification front in a longitudianl cross-section at the center of the laser track (left) and the shape of ripples at the laser track surface from a top view (right) **[3]**.

Since the direction in which the solidification front moves is locally along the maximum thermal gradient, which is normal to the solid–liquid interface, this velocity U_s depends on location and is directly linked to the laser beam velocity U (or the scanning speed S). During solidification the solidified clad acts as a heat sink and solidification is directional. Therefore, interface structures may vary from a planar shape formed at low growth rates to cellular and dendritic shaped. Dendrites are characterized by the growth of trunks and branches along preferred crystallographic orientations **[3]**.

The microstructure development in the track also depends on the solidification behaviour of the melt pool. The principles of solidification control the size and shape of the grains, segregation, and the distribution of inclusions and porosity [11].

Overlapping of the beam can cause different growths. Low overlap ratios often cause a strong discontinuity in grain growth at the neighbouring track interfaces. As opposed to higher overlap ratios, which result in a gradual tilt in grain growth direction towards the succeeding track for a relative beam. This tilt is bigger towards the surface of the coating. [1]

1.4 Goal of this research

Models can aid in understanding of the cladding geometries and process quality in a more time saving and therefore less costly manner than to go through the entire process of clad, preparation, measurement and analysis of the coating. In previous research the prediction of the geometry for a single layer coating of Höganäs 3533-00 powder laser cladded onto a SS304 bar with ø40mm has been successful with a recursive model [5]. This model has been further expanded to multilayer modelling using either laser parameters or single track dimensions [7].

Numerous interactions increase complexity of modelling the geometry. Research data can be used to select corresponding main processing parameters to geometries and microstructural characteristics of real coatings. A further understanding of the consequences of input parameters and cladding procedures can increase and ensure quality of laser cladded coatings. In this research these main influential parameters are identified using empirical data of single layer and multilayers to verify the recursive multilayer model.

Finally, the microstructure of the produced clads will be investigated. Using EBSD several clads are analysed to visualize the grain growth orientation within complete coatings. This will show any relation between laser process parameters and the microstructure of laser cladded coatings.

2 Methods

2.1 Laser cladding process

Before cladding the stainless steel bar (SS304) with a diameter of 40 mm is sandblasted. The laser used for the cladding is a solid state laser: Rofin-Sinar 2kW Nd:YAG. The powder feed system consists of a Sulzer Metco Twin 10C powder feeder with side and coaxial nozzles. As shielding and carrier gas argon is used and hopper #4. The powder used for cladding is Hogonas 3533-00, stainless steel powder for laser cladding. All clad tracks are cladded on a cylindrical stainless steel bar (SS304). The side cladded tracks are cladded on a bar with a diameter of 40mm with an angle of 8˚ to the laser track and the coaxial cladded tracks on a bar with diameter of 38mm and a 25˚ angle to the laser track.

The scanning speed is kept constant at 5mm/s for all clads. Powder feeding rate is 83.3mg/s and 60mg/s and laser power is 600W and 675W. For every coating first a single track is cladded as a reference for the dimensions. After a successfully cladded single track, i.e. no detachment, stable feeding, and smooth surface a single, double or triple layer coating is cladded.

2.2 Sample preparation

To be able to view the laser cladded samples under the microscope, the bar is cut in slices where the tracks propagate along the perimeter of this circular slice. These slices are then cut perpendicular to the cladding propagation so that the cross-section of the coating is visible. The cut samples are mounted inside a conductive mount made of Bakelite. This mount makes it easier to put the sample in a holder for the microscope and the conductive copper makes it suitable for EBSD.

For rough analysis of the geometry with the optical microscope it is sufficient to only do the first few rough polishing steps. To use EBSD the full polishing sequence is necessary (Table 2).

Table 2. Full polishing procedure before EBSD analysis. For optical measurements the first three steps were sufficient. [5]

Polish step	Disc	Time [min]
100 - 200	Sanding discs	5
220	MD-Piano	30
1200	MD-Piano	30
9µm	MD-Largo	45
3µm	MD-Mol	45
Silica OP-U 1µm	MD-Chem	45

2.3 Optical microscopy

For this research an Olympus Vanox-T microscope is used. It is necessary to stitch several separate images together into one to view the full-width image of the coating cross-section. Several distances are measured: height of the dilution for determination of the clad quality and total maximum height and width of the clad coating (Fig. 12). All the heights are measured at least at two different places: the start and end of the clad (left and right of the coating cross-section).

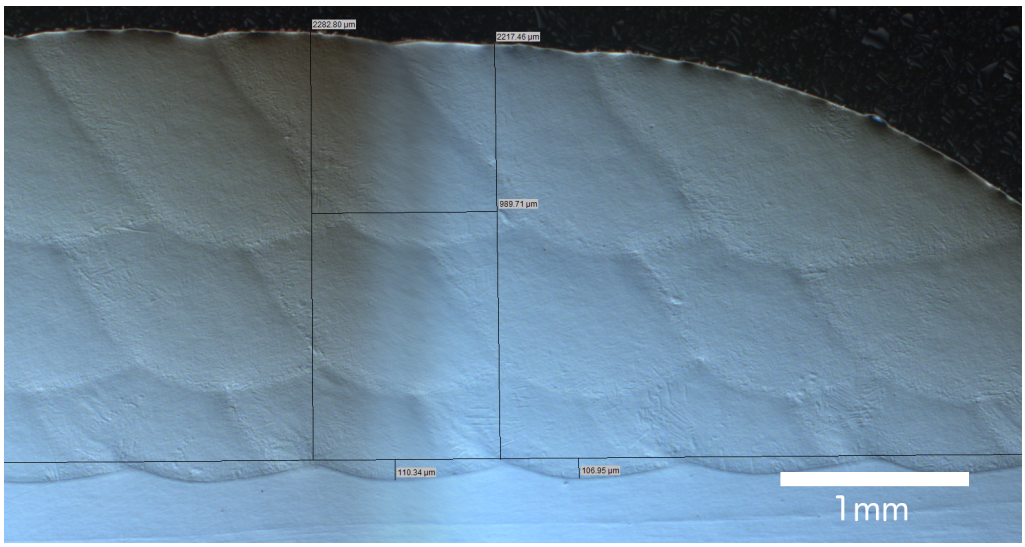

Fig. 12. Side cladded multilayer coating cross-section with indicated properties.

Polarization during viewing is used to make more defined and detailed images. This way, track boundaries are more visible, which will be beneficial for qualitative analysis. This method causes the colouring to the images.

2.3.1 Single track

The maximum width and height of the first single track are measured with the optical microscope as shown in Fig. 13. These properties are then used as direct input in the geometric model using the overlap method.

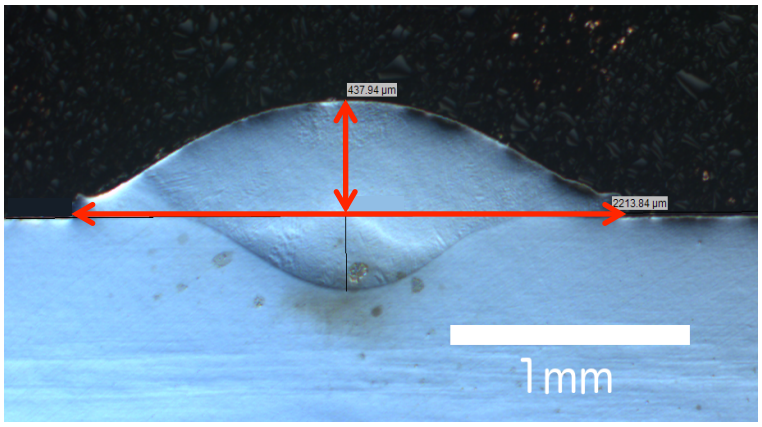

Fig. 13. Side cladded multilayer coating cross-section with indicated properties.

2.4 Overlay of model and experimental images

The geometric model outputs a complete coating with one or multiple layers depending on the wanted total number of layers. For both models (overlap and laser parameter) the output figure is analysed by using the modelled coating (Fig. 14) as an overlay for the experimental images as shown in Fig. 15. This overlay can easily be executed by using graphical software (e.g. Adobe Photoshop).

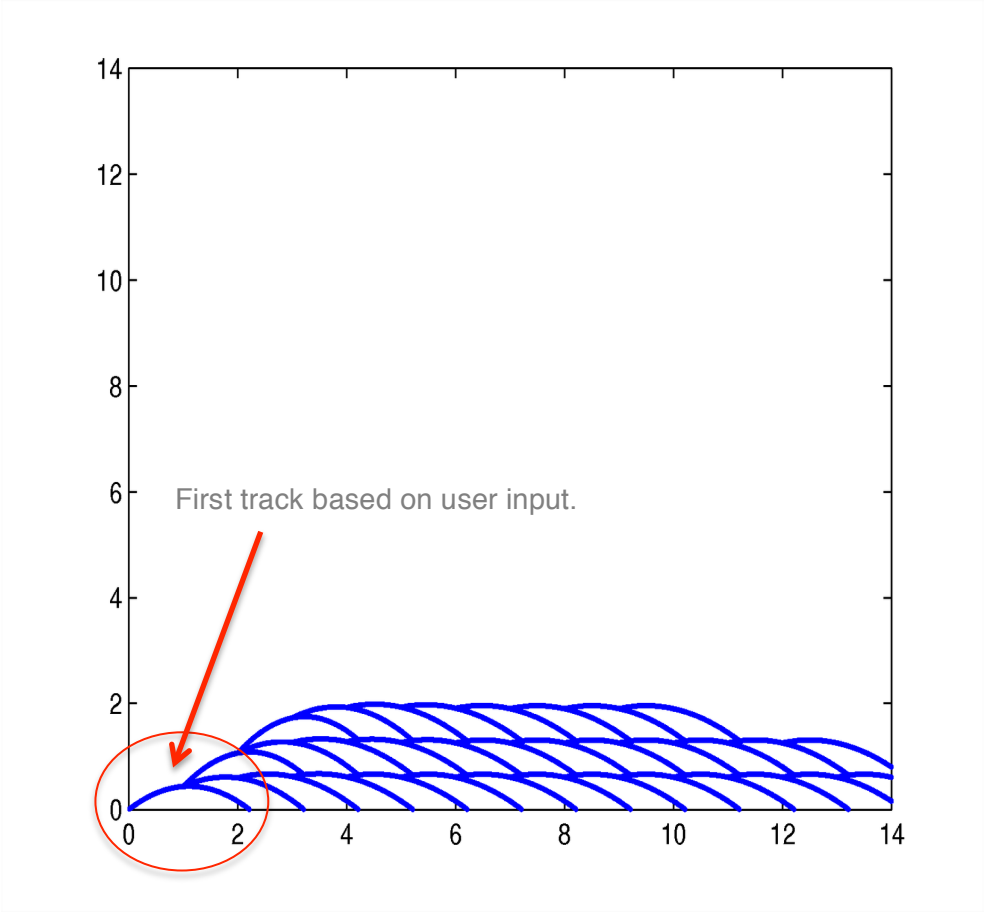

Fig. 14. Output figure of overlap model for a triple layer. Units for both axes are millimetres. H = 0.43749 mm, w = 2.21384 mm, D = 1 mm, Offset = 1mm.

The models use either the laser parameters or the track shape dimensions as the input to render the first track. Using the graphical software this first track, which is highlighted in Fig. 14, is isolated and used as a specific overlay for the experimental single cladded track for qualitative analysis of the initial input of the model. For the overlay of the whole coating the graphical software is used to eliminate the excessive amount of tracks modelled by the program. An example of the resulting overlay image for qualitative analysis is shown in Fig. 15.

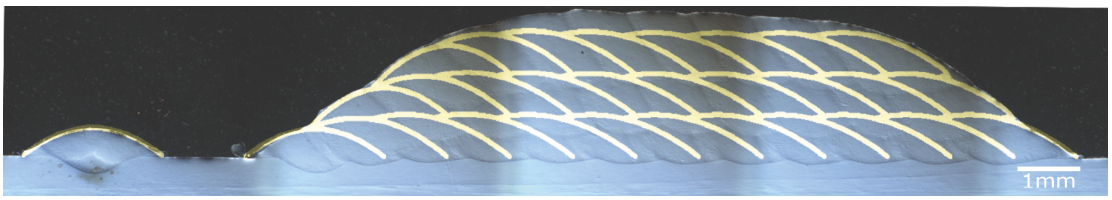

Fig. 15. Experimental cladded triple layer with a overlap model overlay shown in a lighter colour. P = 675W, F = 83.3 mg/s, S = 5mm, D = 1mm, Offset = 1mm.

The above-described overlay method is possible for both the overlap model and laser parameter model. As the dimensions of the experimental single track are measured and used to calculate the single track shape for the modelled coating. Also for the laser parameter model it is possible to make an overlay of the single track, because the coating is modelled using the laser parameters that relate to the dimensions of the track shape as previously discussed in section 1.1.2.

2.5 ESEM & EBSD

An Edax TSL system together with a Philips XL30 ESEM with rotatable sample platform is used to collect OIM data. Using 20keV and 25keV and a spot size of 4 and 5, respectively. The sample stage is tilted by 73˚ degrees towards the CCD camera. With the collected data the OIM Analysis software visualises the crystal orientation of the sample.

2.5.1 Microstructure

Grain boundary lines presented in the OIM data figures are constructed electronically using the criterion that a grain boundary between two points exists when the crystal orientation angle between these two points exceeds 5˚ **[3]**.

It is expected that the directions of grain elongation correspond to the growth direction, because the main heat transfer during solidification is perpendicular to the solidification front.

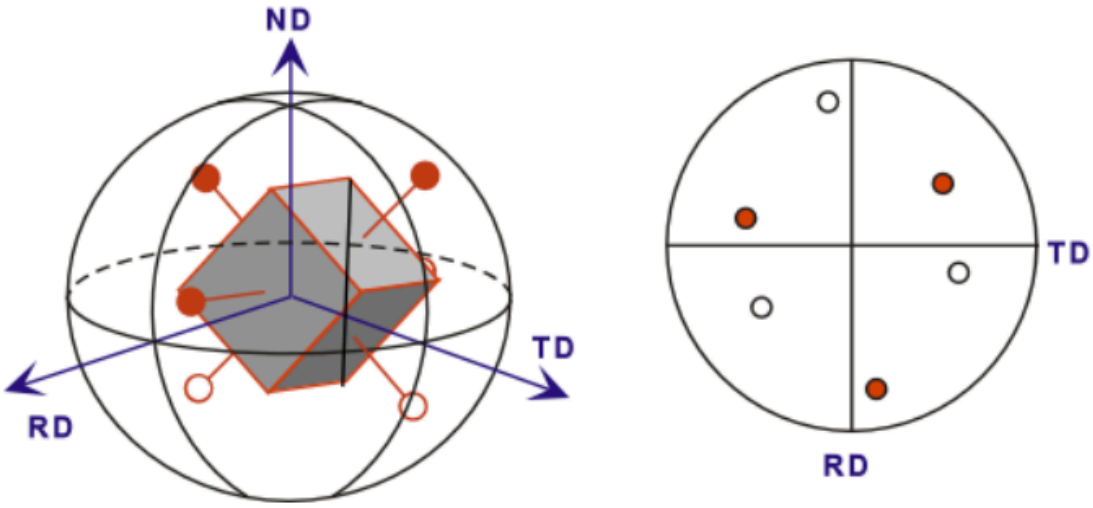

Fig. 16. Hemispherical representation of pole figure points that correspond to the crystal plane directions. [12]

Pole figures (PF) are most common source of texture information in material X-ray analysis. Each PF is equivalent to a geographic map of a hemisphere (North pole in the centre) as shown in Fig. 16, which is formed to connect a line from the South pole to the point on the surface of the northern hemisphere. The intersection of the line with the equatorial plane defines the project point. The equatorial plane is the projection plane. [9]

In Inverse Pole Figure (IPF), we focus on a specific sample plane such as the normal direction (Fig. 17), and find which crystal plane is parallel to this specified sample plane. This crystal direction is then plotted as a stereographic representation on the IPF. Using colours to highlight the difference in accumulation about specific directions.

In OIM Analysis software, the Inverse Pole Figure Map is also used alongside the IPF and legend to show the positions and directions of individual sample grains relative to the sample reference frame shown in Fig. 17. These figures and maps are used for insight in the difference of orientation between tracks and layers of the transversal cuts. Nothing can be concluded about grain growth orientation differences along the track itself, longitudinal cuts would be the necessary method for such an analysis.

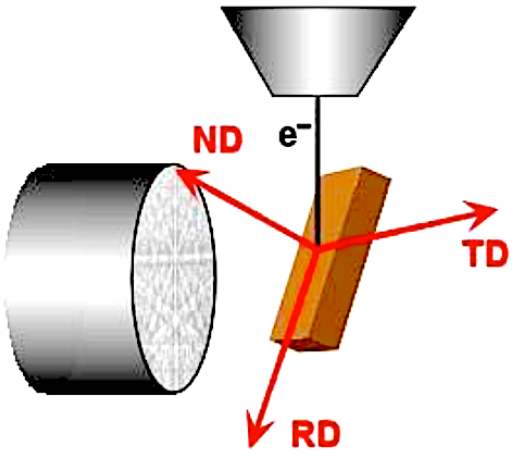

Fig. 17. Schematic overview with specified directions w.r.t. sample coordinates: ND - normal direction, TD - transverse direction, RD - rolling direction. [12]

Each point on an IPF map is coloured according to an automatically colour coded unit triangle of the IPF, also referred to as a legend for the corresponding IPF as in Fig. 18. For example, using the legend the colour red is assigned to the [001] crystal direction, blue to [111] and green to [101]. Shading each point in the OIM scan according to some parameters reflecting the crystallographic rotation generates an orientation map. Crystals with their [111] axis normal to the surface of the sample will be blue as shown in the legend. If a point in the scan is oriented such that the crystal direction aligned with the specified sample direction is somewhere between [001] (red) and [111] (blue) direction (i.e. [112]), then the point would be shaded in purple.[9]

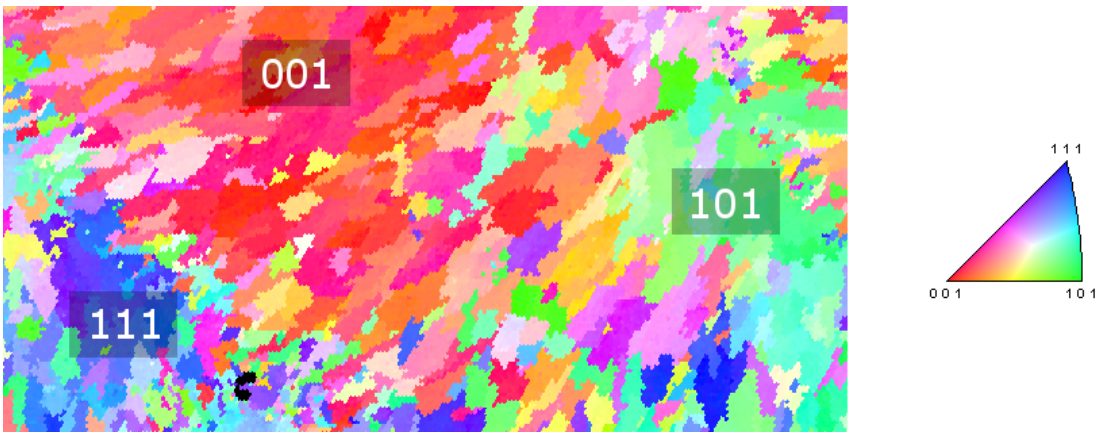

Fig. 18. Partial double layer clad scan IPF map with multiple crystal orientations (left). IPF legend (right).

Since the grain growth is expected to be perpendicular to the solidification front, the normal direction (ND) of the sample will not immediately show definitive preferential crystal orientation when an IPF is rendered. In order to transform the reference basis of space to the reference basis of the crystal structures, the crystal orientation in space is defined by three rotations around RD, TD, and ND. These rotations will give an accumulation of poles about specific directions relative to the sample reference frame. This rotation is done in the OIM analysis software. In essence, we are now looking at a plane perpendicular to the grain growth direction, which in turn is perpendicular to the solidification front.

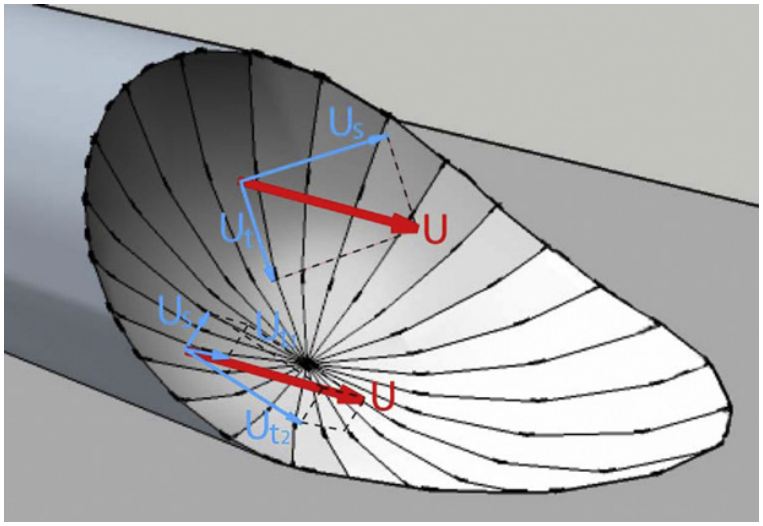

Fig. 19. A sketch of the shape of the solidification front in 3D and local components of grain growth directions U_s at two different point on this front **[3]**.

Together with the IPF maps, which give a visualisation of how crystal structure is orientated in the observed surface and where these orientations occur and accumulate, there are also aspect ratio maps with plots and grain shape orientations maps with plots generated in the OIM analysis software.

Aspect ratio maps show with certain colour shading how large the ellipticity of the grains is. Ellipticity is defined as the lengths ratio of the major and minor axis of an ellipse. If the ellipse is very elongated the ratio will go to 0, as opposed to a circle, which has a ratio of 1. For grains that show in the TD-RD plane, these aspect ratio mappings will help roughly define locally in which direction grain growth occurs with respect to the ND of the sample. Grains that grow perpendicular to the ND will appear more circular than grains that grow at an angle to the ND. There is no

information if this grain tilt is more towards the RD or TD as the ratio is calculated only by lengths and not by directions. The tilts could be occurring in any direction around, as they are pointed away from the ND direction. For the purpose of directional analysis grain shape orientation maps and figures have also been made.

Grain shape orientation maps also use colour shading with purpose to define the grain orientation. Again the grain shapes are identified to have major and minor axis. The mapped orientation angle is that of the major axis in reference to the horizontal of the scanned image. The angles are defined in a clockwise manner as shown in Fig. 20. Where a low angle corresponds to blue and going to a higher angle corresponding to red. Using this scale from a minimum of 2˚ to a maximum of 180˚ the grain shape orientation maps will give an overview of how grains propagate away from the ND axis.

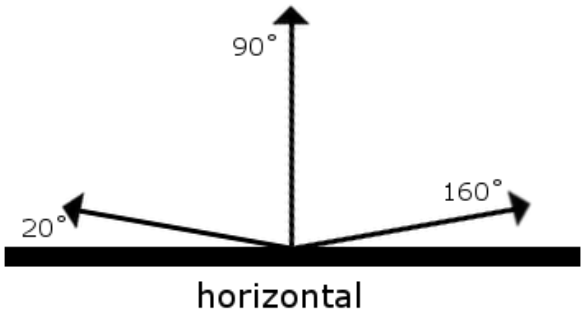

Fig. 20. Major axis orientation and corresponding angles.

Analysis

2.6 Geometric model

2.6.1 Basic principle

To know how well the geometric model for multilayer laser cladded coatings predicts the width and height of a coating, the measured properties were used to calculate the overlap ratio. Together these values served as input for the geometric models. After which the model output figures were compared to the optical microscopy pictures by image overlay. Also the output values for the maximum height have been compared to the measured values. In this report only a few representative and outstanding data will be shown. The complete dataset is in possession at the Material Science department of the University of Groningen.

2.6.2 Overlap model

2.6.2.1 Side cladding

Fig. 21 to Fig. 25 show some of the resulting images by overlapping the overlap model output figures with the microscope images for the side cladded coatings. Where Fig. 21 and Fig. 22 show single layer coatings, Fig. 23 and Fig. 25 depict double layers and Fig. 24 a triple layer coating.

The coating shown in Fig. 21 was cladded with an unstable feeding. However, the width and height match with that of the model as can be seen by the overlay. Since the overlap model depends on the measured dimensions rather than the laser parameters it is no surprise that even such an unwanted cladded coating is predicted quite well.

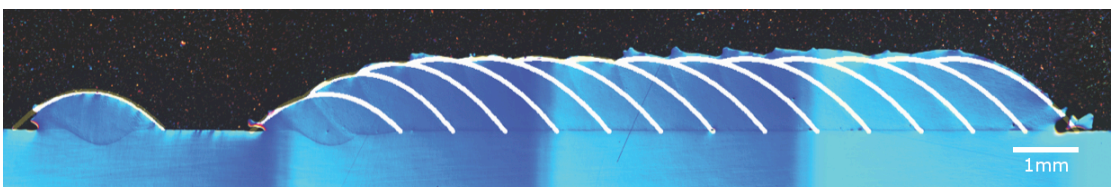

Fig. 21. Experimental single layer side clad compared to model prediction of the overlap model shown as a light-coloured overlay. P = 675 W, F = 83.3 mg/s, S = 5 mm/s, D = 0.8 mm.

For single layer clads (Fig. 21 and Fig. 22) the overlap model gives a realistic geometric figure compared to the experimental cladding. There is a slight discrepancy in the height of both these overlays that could be due to the raggedness that adds to the roughness of the surface where in contrast the model gives a perfect smooth parabola.

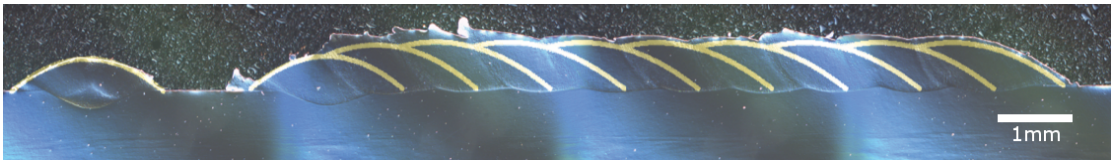

Fig. 22. Experimental single layer clad compared to model predictions by the overlap model shown as a light-coloured overlay.
P = 675 W, F = 83.3 mg/s, S = 5 mm/s, D = 1 mm.

When moving on to multilayer clads (such as shown in Fig. 23 to Fig. 25) the discrepancy in the height becomes more apparent with every extra cladded layer. The modelled height error behaves cumulatively with the number of layers. Also, it is interesting to notice that the height of the model is lower than the actual sample height for all samples that where cladded in a stable and the usual continuous manner.

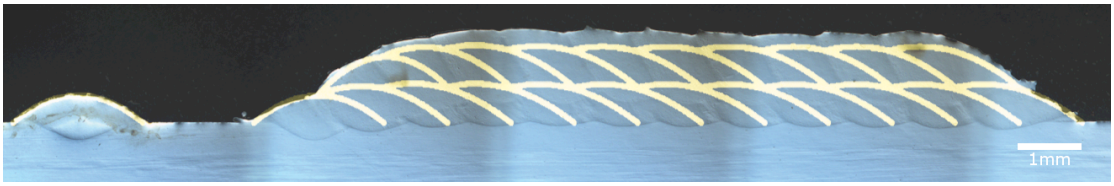

Fig. 23. Experimental double layer compared to model predictions by the overlap model shown as a light-coloured overlay.
P = 675 W, F = 83.3 mg/s, S = 5 mm, D = 1 mm, Offset = 1mm.

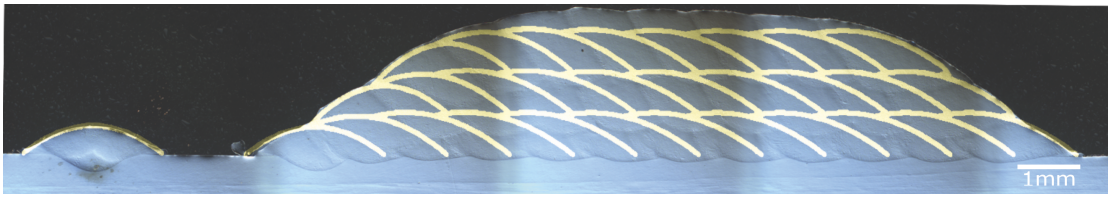

Fig. 24. Experimental triple layer compared to model predictions by the overlap model shown as a light-coloured overlay.
P = 675 W, F = 83.3 mg/s, S = 5 mm/s, D = 1 mm, Offset = 1 mm.

Another sample using the same parameters was made, but in this cladding a pause was inserted in the cladding process. First, a single track was cladded and a first layer immediately after. Then the process was paused. During this break the sample was left to cool a few degrees. Now the second layer was cladded on top of this cooled first layer. This heat loss resulted in a lower build-up in the height of the second coating as seen in Fig. 25. The powder is less efficiently deposited as a molten clad as the previous layer is less warm and re-melts slower. The overlay shows this inefficient deposition as the model has a larger height than the actual experimental clad.

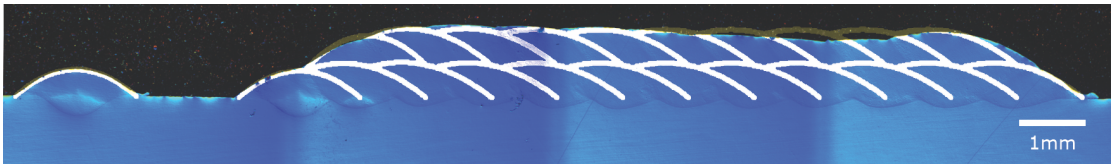

Fig. 25. Experimental double layer side clad compared to model predictions by the overlap model shown as a light-coloured overlay. Sample left to cool between cladding of the first and the second layer.
P = 675 W, F = 83.3 mg/s, S = 5 mm/s, D = 1 mm, Offset = 1mm.

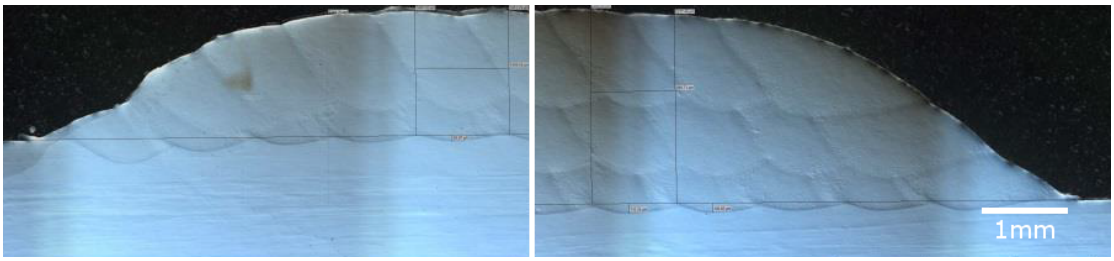

Fig. 26. Comparison of a double (left half) and a triple layer (right half) from Fig. 23 and Fig. 24. Consecutive layers behave the same as other consecutive layers, but different from the first layer. This is true for both coatings shown.

It has already been concluded in previous research [5][7] that the difference in height between model and experiment is because the third assumption of the overlap model is not valid. This means that each successive layer does not have an equal amount of material deposited.

Also the new surface on which is cladded is not as smooth as the SS304 bar surface, but very much more wavy. This waviness, or roughness, can cause the material to be deposited higher than for a smooth surface. Which will result in a larger coating

height. The growth of the total coating height behaves cumulative with every consecutive layer cladded on top.

When the first layer is cladded, the substrate bar is usually still at room temperature. At the time the second layer is cladded, the bar has a significantly higher temperature than before and also the first layer is still warm from being cladded. This heat will affect how well the laser beam re-melts the previous layer when cladding a new layer, as is also the case for the cooled sample in Fig. 25.

How much the laser beam will re-heat a previous layer depends on the thermal capacity of the material of that previous layer. Since the SS304 and the cladded Höganäs 3533-00 are different materials, they will have different heat capacities. This will cause the materials to heat up at different rates when heated by the laser beam.

Therefore these successive layers have a different material behaviour, since they are deposited on another layer, instead of the SS304 substrate. In other words, as can be seen in Fig. 26, the material that behaves as the new substrate after cladding the first layer is the cladded Höganäs 3533-00.

In all cases, for single and multilayer cladded coatings, the total width of the experimental coating is matched by the model overlay. The overall parabolic shape of the model matches the experimental surface roughness, but the more detailed roughness by unstable cladding is not matched.

2.6.2.2 Coaxial cladding

The same overlay method was used for the coaxial cladding results. Fig. 27 to Fig. 29 show some of the resulting images by overlapping the overlap model output figures with the microscope images for the coaxial cladded coatings.

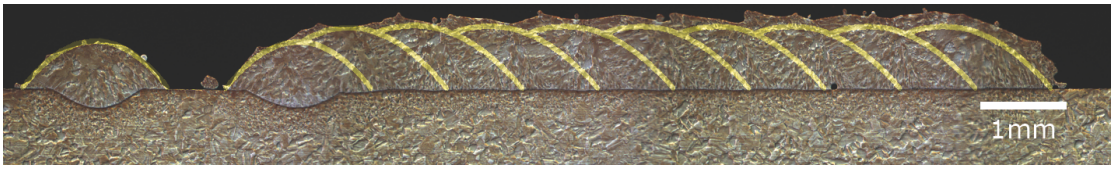

Fig. 27. Experimental single layer coaxial clad compared to overlap model predictions shown as a light-coloured overlay.
P = 600 W, F = 83.3 mg/s, S = 5 mm, D = 0.9mm.

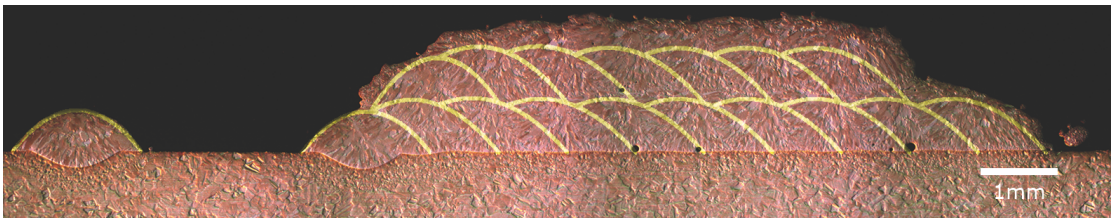

Fig. 28. Experimental double layer coaxial clad compared to overlap model predictions shown as a light-coloured overlay.
P = 600 w, F = 83.3 mg/s, S = 5mm, D= 0.9 mm, Offset = 0.9 mm.

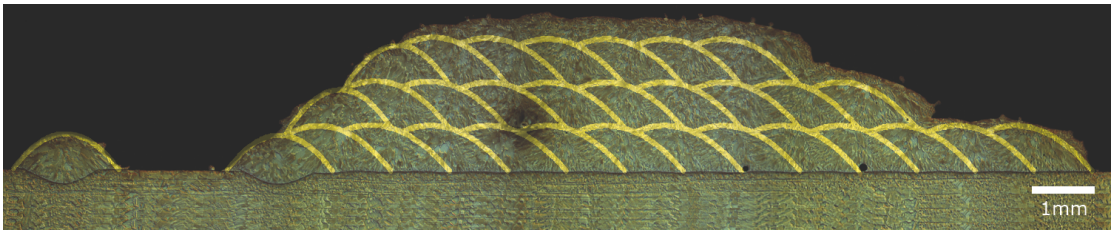

Fig. 29. Experimental triple layer coaxial clad compared to overlap model predictions shown as a light-coloured overlay.
P = 600 W, F = 83.3 mg/s, S = 5 mm, D = 0.9 mm, Offset = 0.9 mm.

For the coaxial cladding the same cumulative behaviour for coating height growth can be observed in the above figures. With each successive layer cladded on to the total coating height is more deviated from the model prediction. Also a slight discrepancy in the width is present, due to unsatisfactory cladding, which resulted in broken edges and a rough surface.

2.6.2.3 Mismatch quantified

The overlays in the previous section give a qualitative result for how much the model matches or mismatches the experimental coatings. For a better judgement there is also a quantitative analysis necessary. Comparing the maximum coating height output of the model with the maximum coating heights measured with the microscope does this. The mismatch between these two values is then defined as the error. This has only been done for the height, since the model interface does not output the total coating width.

The error for the mismatch seen in the overlays is defined as a percentage error using the measured maximum height of the total coating as the reference value. The percentage error can then be calculated as follows:

$$\%_{error} = \frac{model - measured}{measured} * 100\%$$

Absolute values are not used, since it is of interest whether the model calculates a coating that is too high or too low in comparison with the experimental coating.

For the measured values there is a random error of +/- 0.05mm as a result of human involvement when observing the optical measurements and deciding where the bottom and top of the coating are. This was found by taking the differences between two coinciding points. This gives a measurement error in the percentage error as follows according to propagation of uncertainties:

$$\Delta\%_{error} = 2 * \left(\frac{\Delta m}{m}\right)^2 + \left(\frac{t}{m}\right)^2 * \left(\left(\frac{\Delta t}{t}\right)^2 + \left(\frac{\Delta m}{m}\right)^2\right) * 100\%$$

Where *m* is the measured value and *t* is the theoretical (here: model) value and Δt and Δm are the measurement errors of these values. Since $\Delta t << \Delta m$ it can be neglected. The total measurement errors are 0.6% and less, therefore they negligible for the calculation of the percentage error.

Table 3. The laser parameters, maximum heights from the model and measurements, and the percentage error for each sample for the overlap model. * Coaxial cladding.

P [W]	F [mg/s]	Nr. of layers	S [mm/s]	D [mm]	Max. Height model [mm]	Max. height measured [mm]	Percentage error [%]
600	60	1	5	1	0.400	0.712	-43.8
600	60	2	5	1	0.730	1.493	-51.1
675	83.3	1	5	1	0.620	0.714	**-13.2**
675	83.3	2	5	1	1.190	1.407	-15.4
675	83.3	3	5	1	1.960	2.250	**-12.9**
675	83.3	2	5	1	1.030	0.910	**13.1**
675	83.3	1	5	0.8	0.270	0.355	-24.0
675	83.3	1	5	0.8	1.120	1.216	**-7.9**
675	83.3	2	5	0.8	2.030	2.217	**-8.4**
600	83.3	1	5	0.9	0.730	0.866	-15.7 *
600	83.3	2	5	0.9	1.380	1.781	-22.5 *
600	83.3	3	5	0.9	2.010	2.368	-15,1 *

Table 3 shows for every cladded coating the laser parameters used to clad and the number of layers. With these values the results can be related to the sample images. For each sample there is a column with the maximum height that the model calculated and a column with the maximum height that was measured using the microscope. The last column holds the calculated percentage errors. These values are negative when the model gives a smaller value for the height than the measured height and are positive when the model outputs a larger value for the height.

There is only one value for the percentage error that is positive, which is marked in red in Table 3. This particular sample has already been discussed in the previous section as the sample with cooling time in the cladding process, and corresponds to

Fig. 25. All other samples have a larger value for the maximum coating height than the model predicted.

Some predictions show a large percentage error. Most of these samples were not cladded to satisfaction or were unstable in some way. A tolerable percentage error would be 15%, which leaves only five model overlays (boldfaced and underlined in the table) that where a match within the tolerated uncertainty for the height of the experimental coating. It can be concluded that overall the overlap model does not match the height of the experimental coating.

In detail, the overlap model fits best for side cladded coatings with following laser parameters: P=675W; F=83.3mg/s; S=5mm/s. There are not enough claddings done to see which overlap ratio fits better, with D=0.8mm or D=1mm.

2.6.3 Laser parameter model

2.6.3.1 Side cladding

Since the input for this model does not regard the height and width of the experimental coating, the overlay of the first track is not matched in all cases, as was with the overlap model. The total width of the coating does match for all side cladding samples. As for the height of the total coating, there is a mismatch as seen for the overlap model predictions. Again, this mismatch seems to be cumulative with every added layer as Fig. 32 to Fig. 34 show.

The cladding sample in Fig. 30 shows a similar result to the overlap model Fig. 25, which has a model prediction which is higher than the experimental sample height.

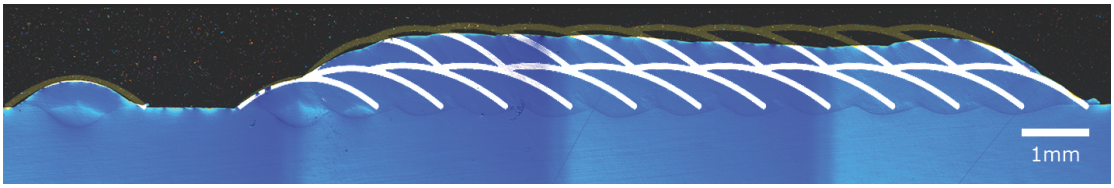

Fig. 30. Experimental double layer side clad compared to laser parameter model shown as a light-coloured overlay. Cooling time between cladding of the first and the second layer. P = 675 W, F = 83.3 mg/s, S = 5 mm/s, D = 1 mm, Offset = 1 mm.

In the next figure, Fig. 31, there is a higher discrepancy than seen in Fig. 21. This shows that the degree of cladding stability is relevant for samples predicted by the laser parameter model.

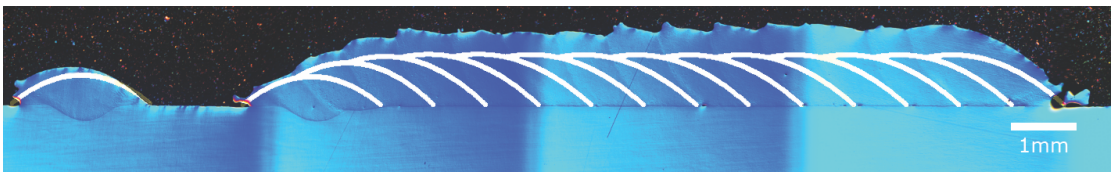

Fig. 31. Experimental instable single layer side clad compared to laser parameter model shown as a light-coloured overlay.
P = 675 W, F = 83.3 mg/s, S = 5 mm/s, D = 0.8 mm.

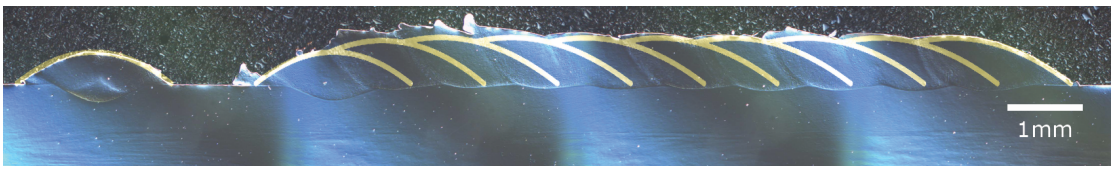

Fig. 32. Experimental single layer side clad compared to laser parameter model shown as a light-coloured overlay.
P = 675 W, F = 83.3 mg/s, S = 5 mm/s, D = 1 mm.

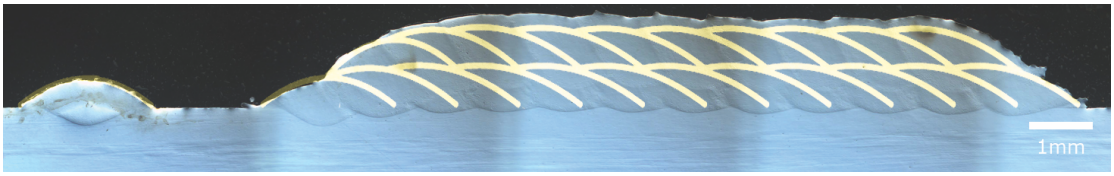

Fig. 33. Experimental double layer side clad compared to laser parameter model shown as a light-coloured overlay.
P = 675 W, F = 83.3 mg/s, S = 5 mm/s, D = 1 mm, Offset = 1mm.

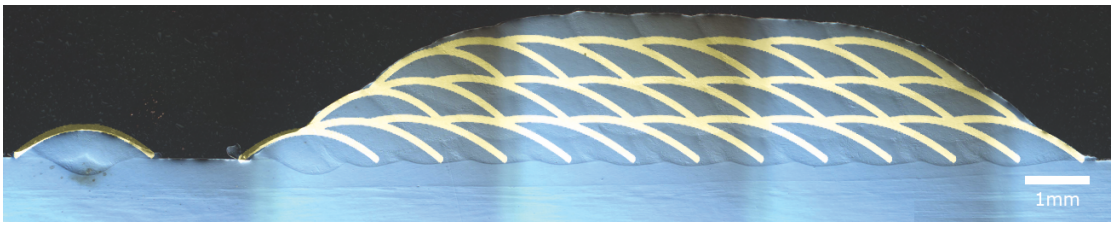

Fig. 34. Experimental triple layer side clad compared to laser parameter model shown as a light-coloured overlay.
P = 675 W, F = 83.3 mg/s, S = 5 mm/s, D = 1 mm, Offset = 1mm.

2.6.3.2 Coaxial Cladding

The experimental constants (Table 1) were determined using a set-up with a side nozzle. This means that the coaxial clads will by definition not match the laser parameter model output resulting from the input used in this research. For every change made in the set-up and materials used, the experimental constants should be determined again. It is extremely tedious to determine the constants for every new combination of set-up, substrate and powder used in in experiments.

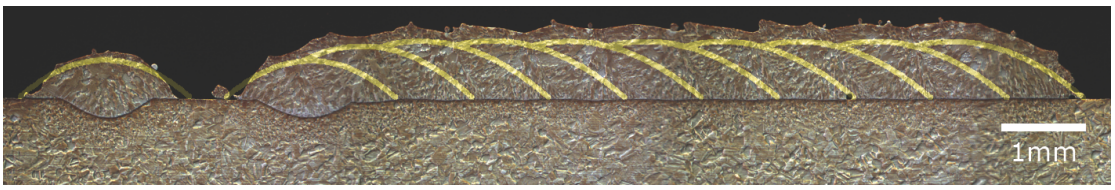

Fig. 35. Experimental single layer coaxial clad compared to laser parameter model shown as a light-coloured overlay.
P = 600 W, F = 83.3 mg/s, S = 5 mm/s, D = 0.9 mm.

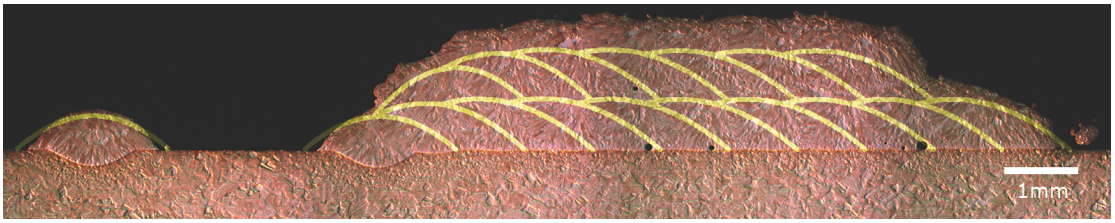

Fig. 36. Experimental double layer coaxial clad compared to laser parameter model shown as a light-coloured overlay.
P = 600 W, F = 83.3 mg/s, S = 5 mm/s, D = 0.9 mm, Offset = 0.9 mm.

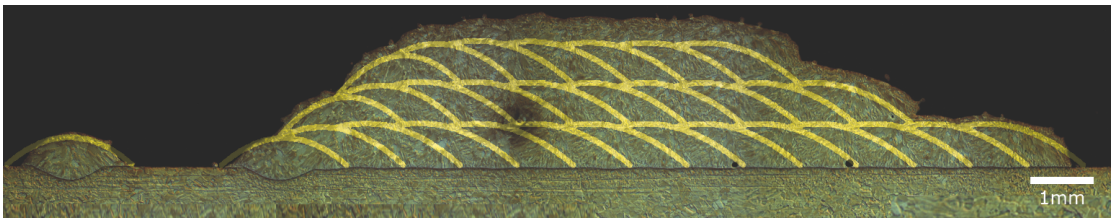

Fig. 37. Experimental triple layer coaxial clad compared to laser parameter model shown as a light-coloured overlay.
P = 600 W, F = 83.3 mg/s, S = 5 mm/s, D = 0.9 mm, Offset = 0.9 mm.

2.6.3.3 Mismatch quantified and discussion

To show quantitatively how well the laser parameter model fits the experimental values the percentage error is calculated. This was done by the same method as for the overlap model. The resulting values are given in Table 4.

For the laser parameter model the values of the $\Delta\%_{error}$ are less than 0.1%, which can also be neglected for this model.

Table 4. The laser parameters, maximum heights from the model and measurements, and the percentage error for each sample for the laser parameter model. * Coaxial cladding.

P [W]	F [mg/s]	Nr. of layers	S [mm/s]	D [mm]	Max. Height model [mm]	Max. height measured [mm]	Percentage error [%]
600	60	1	5	1	0.400	0,440	-38,2
600	60	2	5	1	0.730	0,870	-41,7
675	83.3	1	5	1	0.620	0,620	**-13,2**
675	83.3	2	5	1	1.190	1,230	**-12,6**
675	83.3	3	5	1	1.960	1,840	-18,2
675	83.3	2	5	1	1.030	1,230	35,1
675	83.3	1	5	0.8	0.270	0,770	116,8
675	83.3	1	5	0.8	1.120	0,770	-36,7
675	83.3	2	5	0.8	2.030	1,530	-31,0
600	83.3	1	5	0.9	0.730	0,650	-24,9 *
600	83.3	2	5	0.9	1.380	1,290	-27,6 *
600	83.3	3	5	0.9	2.010	1,740	-26,5 *

For this model the same tolerance of 15% is used to see which overlays fit the measured values. This gives only 2 overlays that fit within the stated tolerance. For the laser parameter model it can be concluded that the model does not fit the experimental values.

The same holds here as for the overlap model. The laser parameter model fits best for side cladded coatings with following laser parameters: P=675W; F=83.3mg/s; S=5mm/s. There are not enough claddings done to see which overlap ratio fits better, with D=0.8mm or D=1mm.

For the purpose of the prediction with the laser parameter model an enormous database would be needed with all the constants for different cladding situations. Therefore, also here the existing possibilities within the model should first be looked at further. This could mean, using the functionality of defining the consecutive layers separate from the first layer. Also adding an extra parameter, such as heat capacity of the materials, should be looked into.

2.6.4 Discussion

Independent of the model type, the height of the clad is mismatched. Overall, the height of the model is always lower than the measured experimental coating height. There are two exceptions in the results for the heights: first, the clad that was left to cool a few degrees during the cladding process, and second an instable cladding. On the other hand, the width and the surface roughness are predicted very well for side cladding.

The difference in coating height could mean that each successive layer does not have an equal amount of material deposited for the experimental cladding. However, the model takes all the inputs and parameters that hold for the first layer and uses them for the successive layers as well. Without accounting for the different materials used. To use the model more realistically the consecutive layers should be treated as new substrates, as the powder and steel bar have different material behaviour, such as their heat capacities.

When it shows that the consecutive layers in all cases are a certain factor higher than the first layer, the model could easily be adjusted. There is a factor present in the models code that can account for height discrepancy. This factor is set at a standard value of 1,00 and can easily be set to another value.

The overlap model has the advantage that it would in theory immediately match the coating since it is based on the geometric properties of the first track of that coating. On the other hand, it is time consuming to have to cut, polish and examine each sample to measure its dimensions.

The laser parameter model would remove the trouble of checking each and every sample for its dimensions. However it needs a lot of research time to set up a database for the values of the experimental constants for each set-up and materials used. This model would also need the samples to be cladded in a stable manner; otherwise the surface will deviate too much from expected clad results.

For more precision the relation between starting temperature of the substrate and the amount of powder re-melting and successfully deposited could also be researched. Since the temperature of the material certainly has an effect on the growth of the next layer on top of the previous layer.

Since the temperature effects and database set-up for the experimental constants are probably more time consuming to investigate, the emphasis for further research should first lie with the input for successive layers in the existing geometric multilayer model, and the effect of incorporating the materials heat capacity for a more realistic model.

2.7 Microstructure

Typical IPF maps and figures are depicted in Fig. 38, Fig. 39, and Fig. 40. The first two figures are scans of the same double layer side cladded sample, but scanned at different locations along the transverse cut. The last figure is of a triple layer coaxial clad. These images are the result of using OIM Analysis software on EBSD data. In the given figures the first image has the separate tracks indicated by a thick black line for visibility reasons. The complete dataset of analysis results is in possession of the Material Science department at the University of Groningen.

When viewing the structure in the ND-direction of the sample reference frame there is significant preferential growth in the [001]-direction, parallel to the ND-direction. This growth direction is located at the centre part of the track and therefore the central area of the solidification front. The location and quantity is roughly the same for side cladding and coaxial cladding.

For both side and coaxial clads viewing from the TD-direction shows grain growth parallel to that direction in the lower-right areas of the re-melted tracks. In Fig. 39 there is a second layer, which consists of less tracks than the first layer. The result is that a non-re-melted track can be seen on this second layer. The grain growth parallel to the TD-direction in the second map is not only positioned in the lower part of the track, but from top to bottom on the right part of the track. This direction also corresponds to the shape of the edges of the solidification front.

The grain growth direction parallel to the RD-direction is not clear from only one image. When comparing multiple figures it is seen that there is grain growth parallel to the RD-direction in the areas where the consecutive layer has re-melted the previous layer. Again this is as expected when seeing that the solidification front has that same area with a surface perpendicular to the RD-direction.

If the distance D is made small enough, the areas left and right of the central part of the track can be excluded by re-melting during the cladding process. This would give a stronger texture when viewing growth parallel to the ND-direction. How large directional growth areas in the transverse cut image are, depends on how much of the area of the full track is viewed. If nothing is re-melted, different preferential growths can be seen from tracks where parts are re-melted.

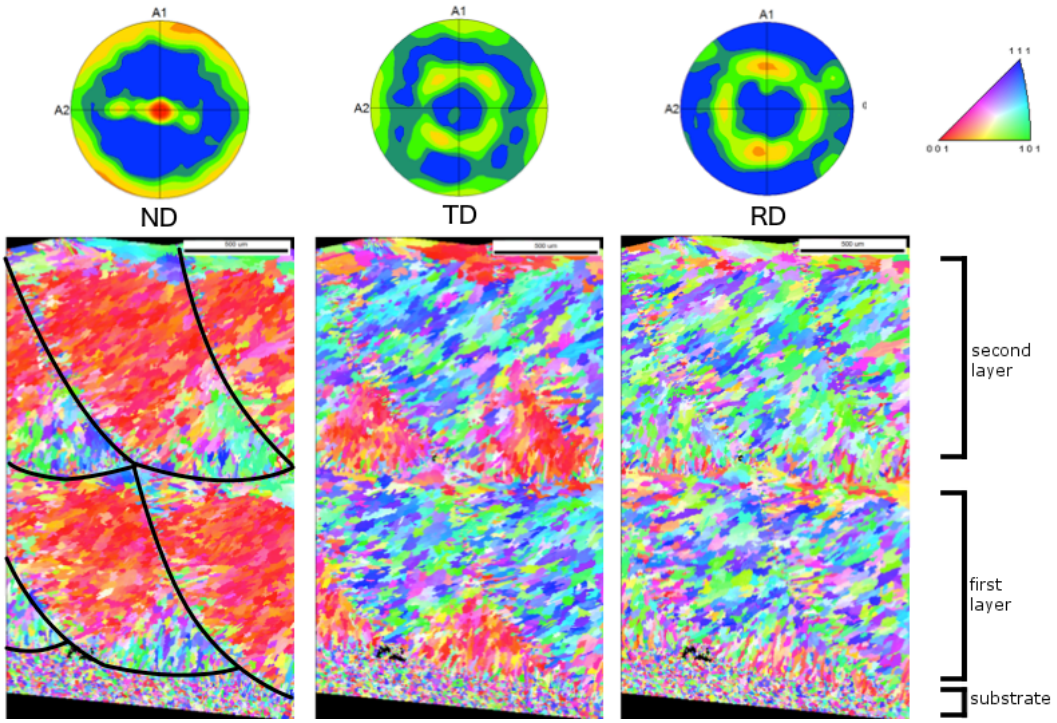

Fig. 38. OIM scan IPF map and figures of a double layer side clad coating.
P = 675 W, F = 83.3 mg/s, S = 5 mm/s, D = 0.8 mm, Offset = 1mm.
Rotations around RD = 48˚, TD = 50˚, ND = 15˚.

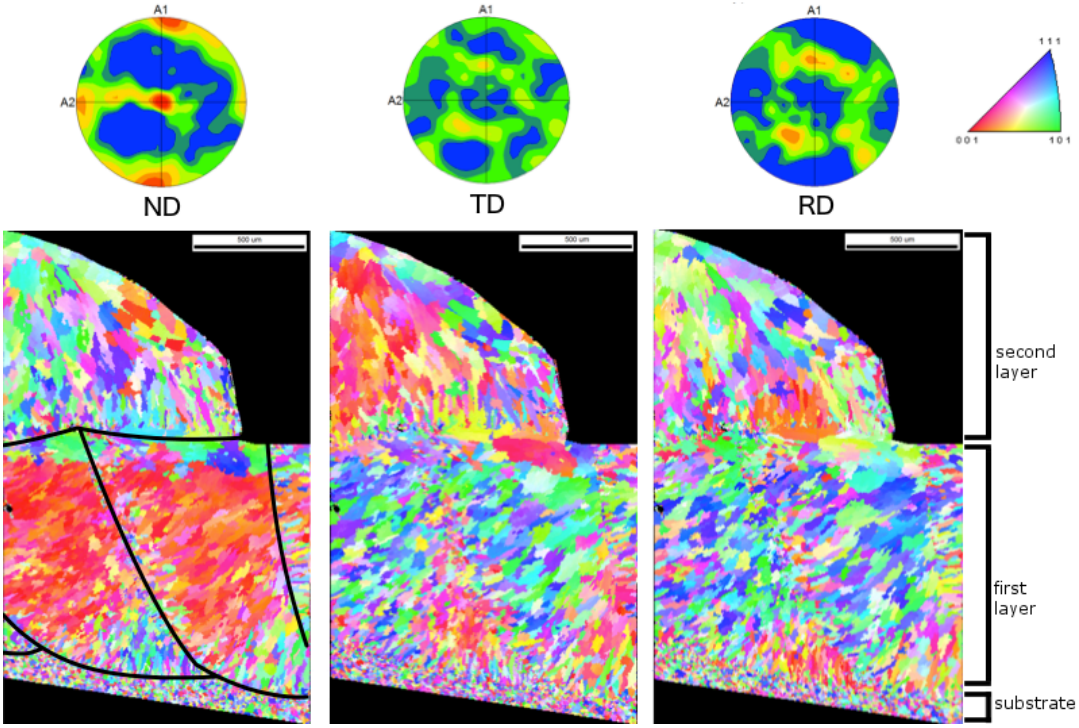

Fig. 39. OIM scan IPF map and figures of a double layer side clad coating. Second layer has less tracks than first layer.
P = 675 W, F = 83.3 mg/s, S = 5 mm/s, D = 0.8 mm, Offset = 1 mm.
Rotations around RD = 55˚, TD = 35˚, ND = 45˚.

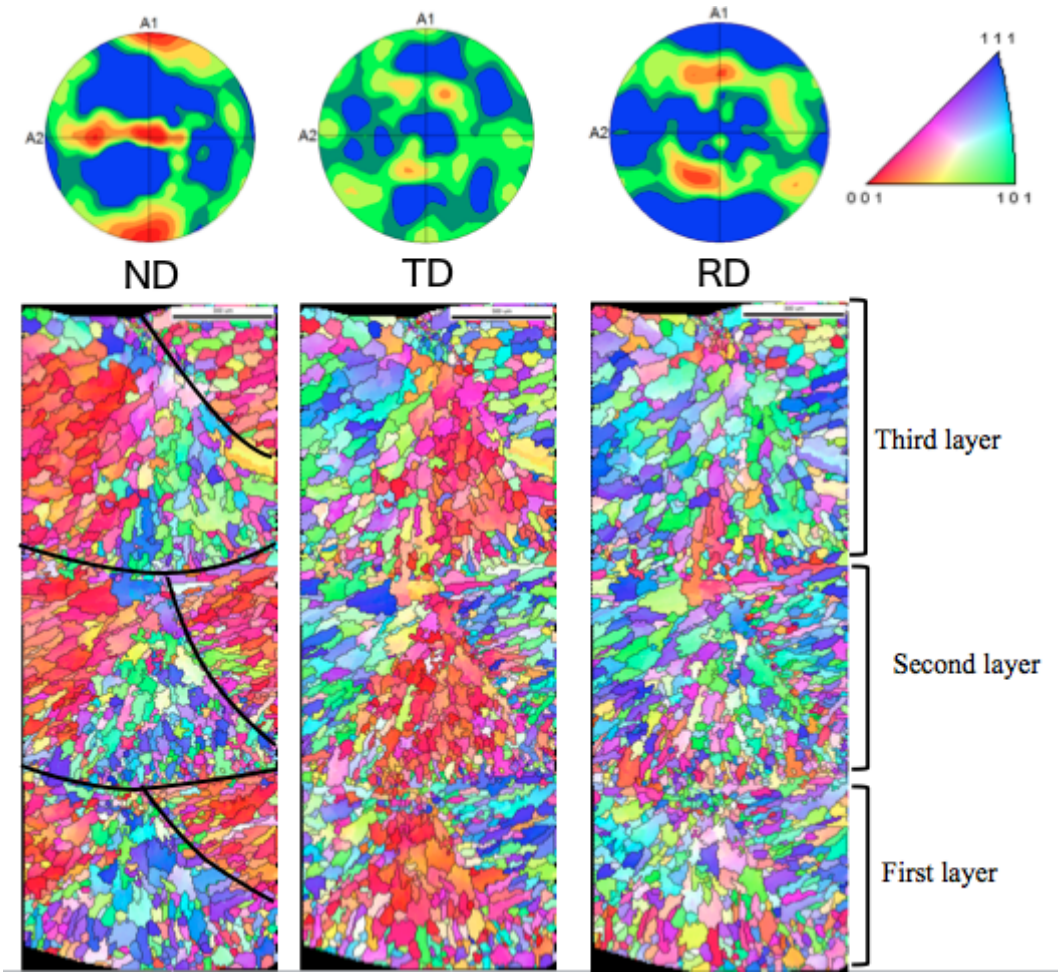

Fig. 40. OIM scan IPF map and figures of a triple layer coaxial clad coating.
P = 600 W, F = 83.3 mg/s, S = 5 mm/s, D = 0.9 mm, Offset = 0.9 mm.
Rotations around RD = 55˚, TD = 30˚, ND = 50˚.

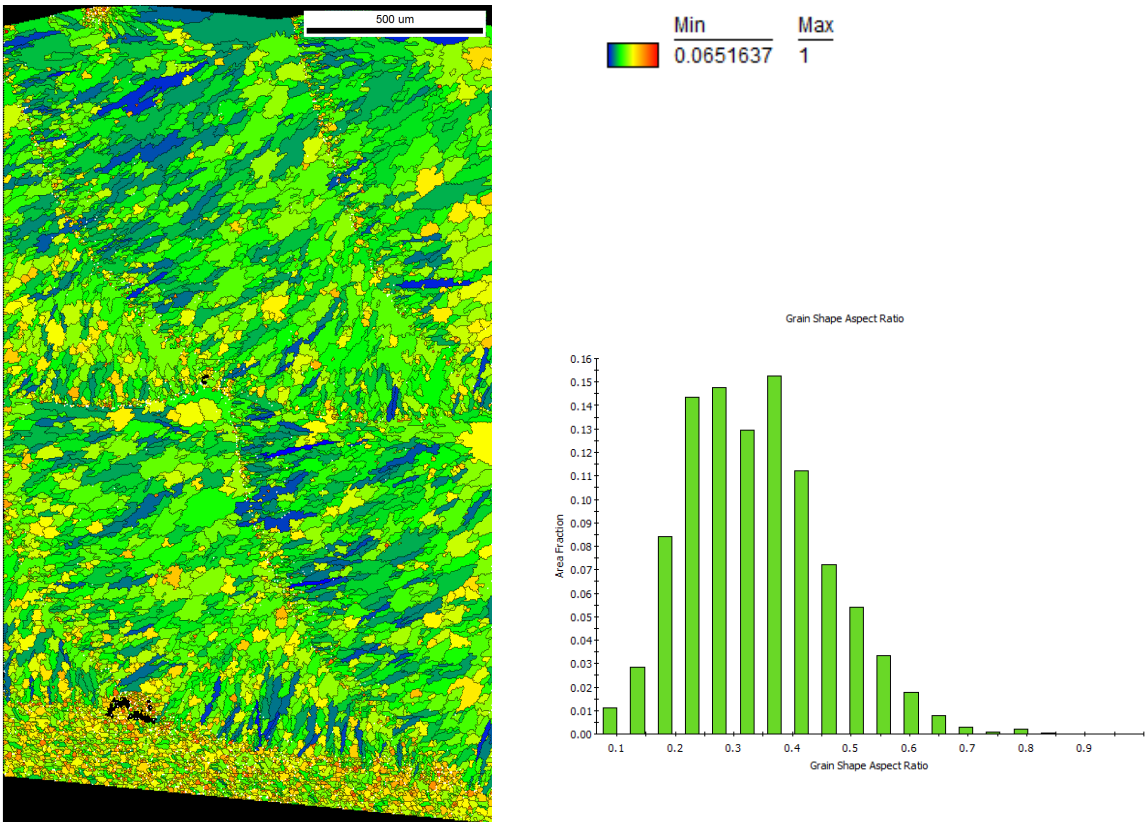

Fig. 41. Grain aspect ratio map and plot for a double layer side cladded coating.
P = 675 W, F = 83.3 mg/s, S = 5 mm/s, D = 0.8 mm, Offset = 1 mm.

Fig. 41 shows the aspect ratio map for the same sample as shown in Fig. 38. What stands out immediately is that the majority of the grains are elongated as opposed to the substrate, which is a mixture of round and elongated grains. This large elongation means that the grains are not perpendicular to the sample surface, but inclined at an angle with respect to the ND-direction. That supports the idea of the grain growth occurring in the direction of the heat transfer. To quantify the elongations also a plot of the grains aspect ratios is made. The average aspect ratio for the side cladded sample is 0.427. The coaxial cladded sample has an average of 0.474. Substrate data is not used in the calculation of this average.

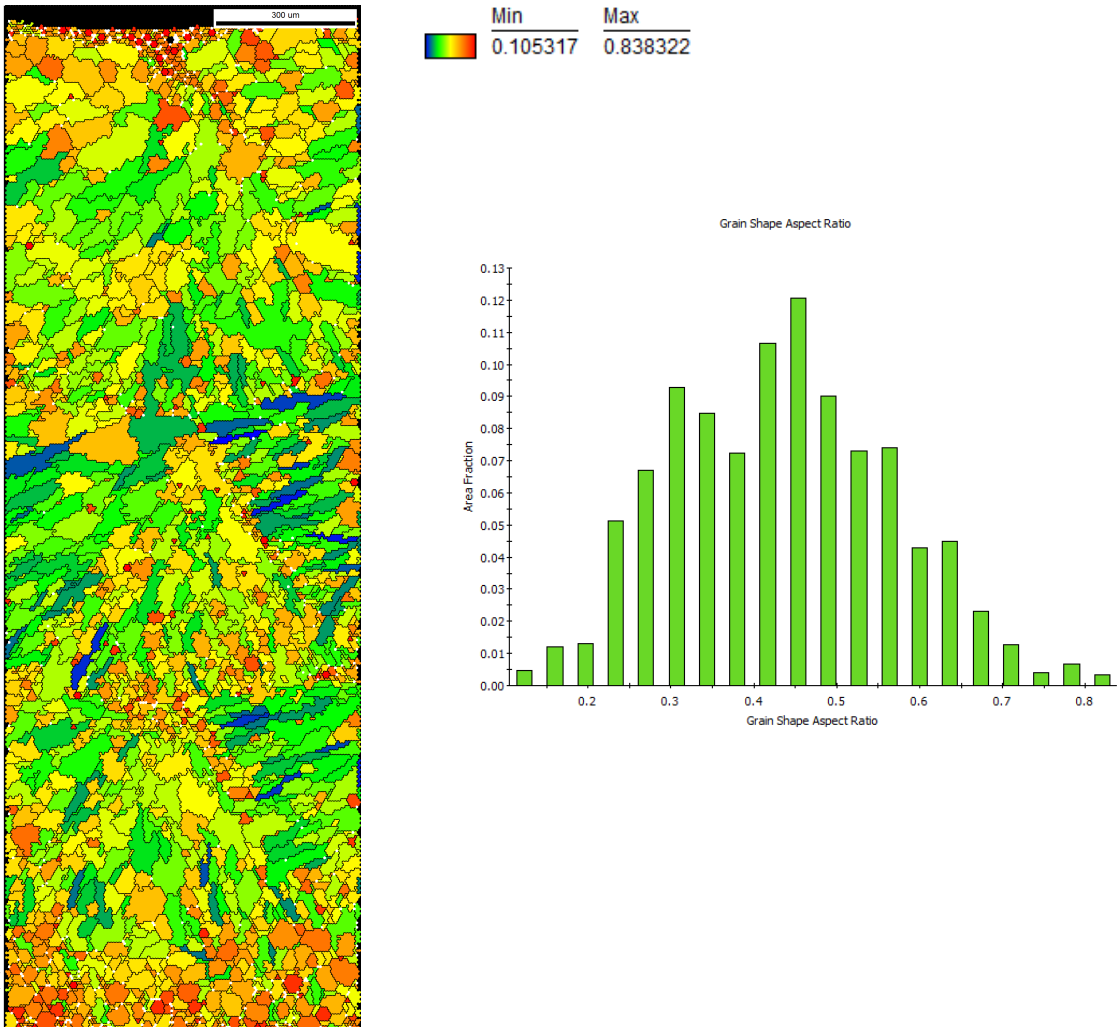

Fig. 42. Grain aspect ratio map and plot for a triple layer coaxial cladded coating. P = 600 W, F = 83.3 mg/s, S = 5 mm/s, D = 0.9 mm, Offset = 0.9 mm.

These plots alone do not show exact in which direction the growth is, but only characterize that there are different directions by seeing elongated images of the grains as they were cut off at an angle with respect to their propagation during the sample preparation.

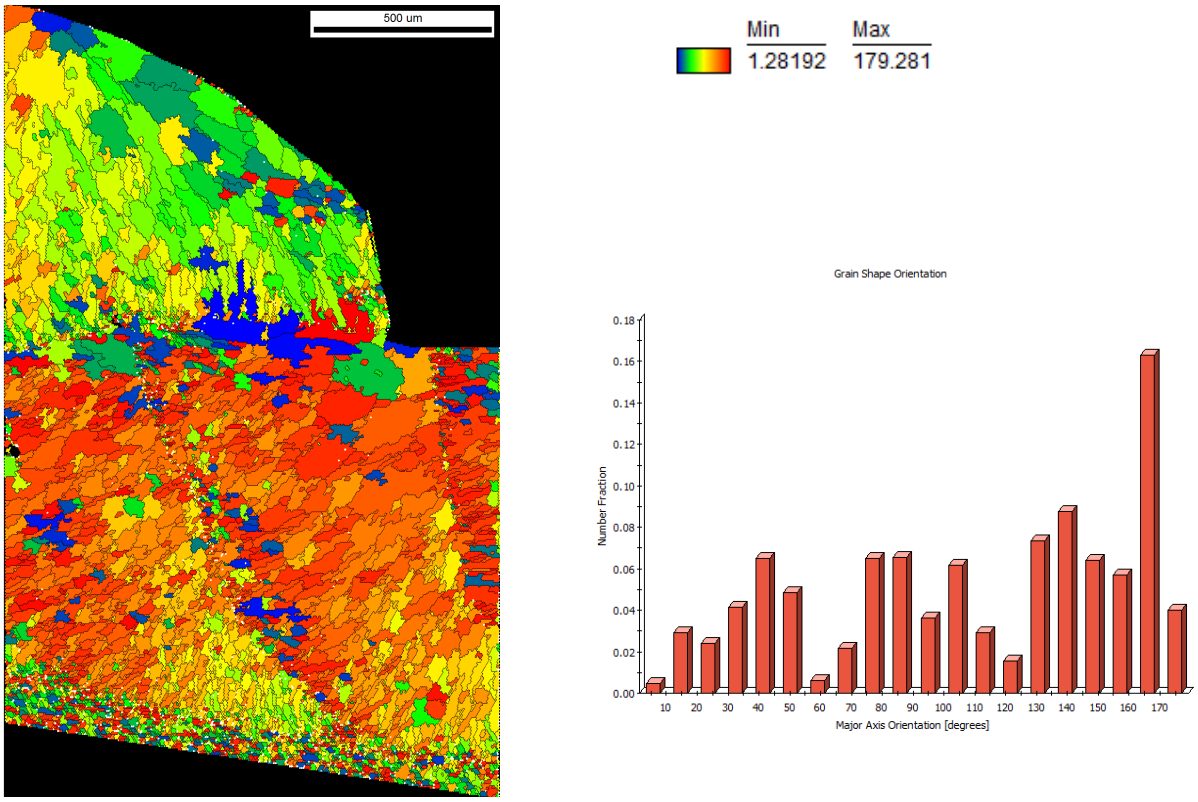

Fig. 43. Grain shape orientation map and plot for a double layer side cladded coating. P = 675 W, F = 83.3 mg/s, S = 5 mm/s, D = 0.8 mm, Offset = 1 mm.

The double layer side cladded sample in Fig. 43 shows distinctive areas of grain growth orientation. The directions with a high angle are grouped around the areas where the grains of a new track grow perpendicular from their solidified neighbour track. Further, the original growth direction of a non-re-melted track can be seen in the track in the second layer. This growth is perpendicular to the substrate surface on which it grows, here the previous layer as also shown in Fig. 44. The same holds for the lower-right area in the track. Due to the overlap of the tracks the orientation in one particular direction is more represented than in the situation if only non-re-melted tracks were to be analysed. The average major axis orientation for the sample in Fig. 43 is 112˚. This is 108˚ for the triple layer coaxial cladded sample in Fig. 44.

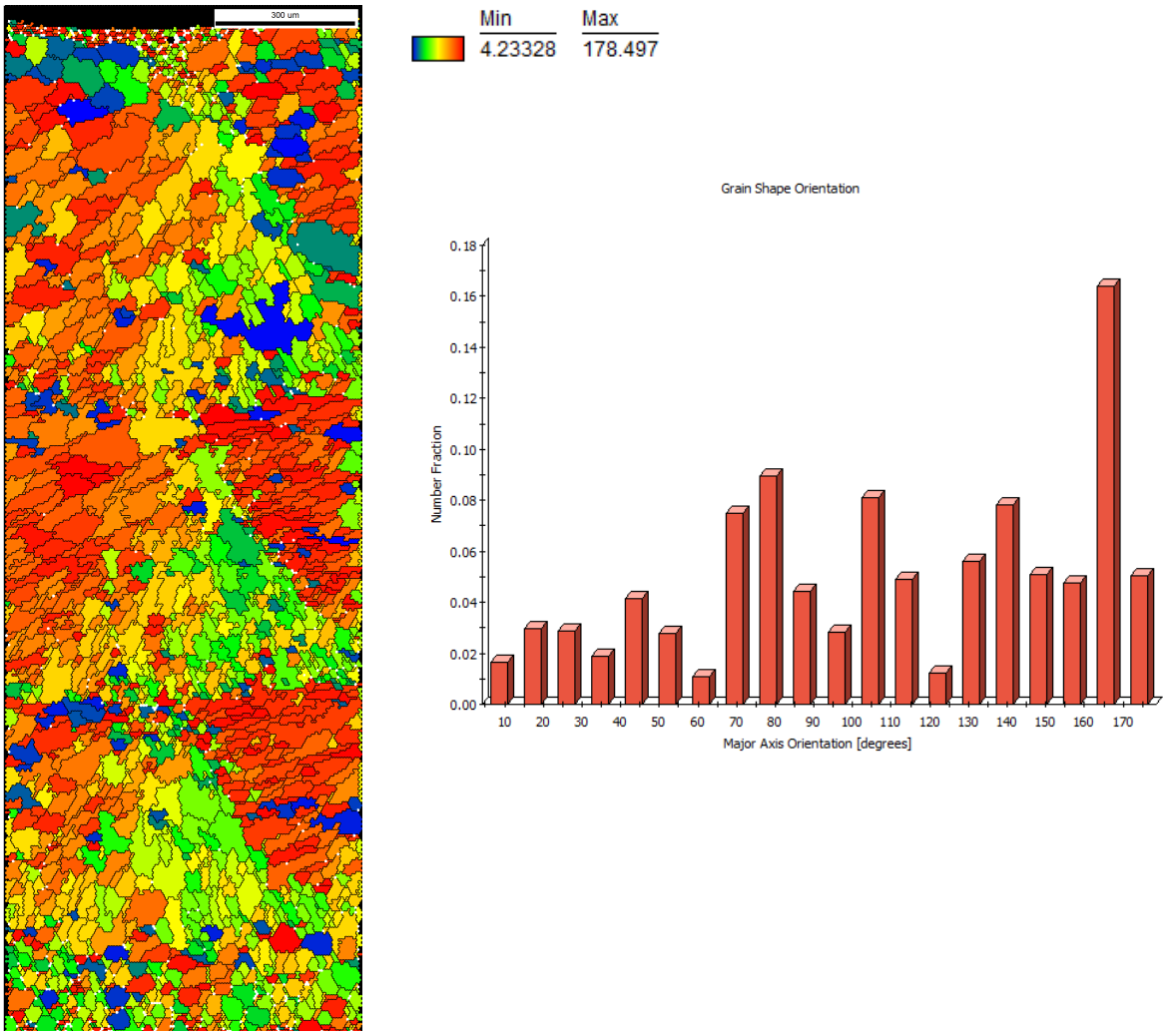

Fig. 44. Grain shape orientation map and plot for a triple layer coaxial cladded coating. P = 600 W, F = 83.3 mg/s, S = 5 mm/s, D = 0.9 mm, Offset = 0.9 mm.

2.7.1 Discussion

There is a small difference in preferential crystal orientation of the grains for a side and coaxial cladded coating. These differences might also be due to interpretation of the image. As seen for the double layer side cladded sample with the visible endpoint of the second layer. When the scan only shows certain parts of the tracks the analysis shows the orientation angles and aspect ratios of only the scanned area. Therefore, the plots and maps should be all interpreted together, and not be separated. Overall, the OIM software can give a good qualitative and quantitative estimation of the preferential grain growth direction in a sample.

Track boundaries have no preferential crystal orientation due to nucleation effects during the cladding process. The substrate bar needs to be removed from the scan image using the OIM software to prevent interference of the data of the substrate and misinterpretation of the resulting maps and plots.

Preferential grain growth direction is seen to depend upon the type of cladding method used, the number layer that is analysed, and the displacement used during cladding. With smaller displacement, less of the total track is shown and the stronger depicted texture is.

3 Recommendations

As was seen in the model verification for multilayer cladded coatings temperature made a difference for the height growth of the layers. If it proves to be highly predictable for the resulting height in any way, interlayer cooling can be a future parameter for the model. For now, it seems more likely that material characteristics are involved, such as the heat capacity. The implementation of such material characteristics should be investigated.

At the moment there is a factor implemented in the Matlab code of the prediction models that is set to 1,00. When this factor is changed, the height of the total coating changes accordingly. This is also a way to research the effect of consecutive layer behaviour during cladding of multiple layers.

For the overlap model to treat the consecutive layers as new substrate for the previous layer the width, height, overlap and offset of the new substrate should be known. A way to do this is to make a single layer coating and a single track on top of this first layer. Then the dimensions can be measured in the same way as for the other single track. At the moment there is already a way to set these parameters at different values for the consecutive layers in the overlap model. However, these settings can only be done for the consecutive layers as a whole. This should not be a problem as the triple layers showed that the third layer behaves the same as the second layer, since they both have a substrate with the same physical aspects. The expectation is that consecutive layers all behave the same.

The same holds for the laser parameter model, where all the laser parameters, the experimental constants and displacement are needed. These can be set at different values for the consecutive layers as a whole and not individually for every layer.

At the moment there is no significant difference between the results of the overlap and laser parameter model. Only for instable claddings it is clear that the laser parameter predicts a more ideal coating than the experimental coating. For the laser parameter model a database would be needed with all the experimental constants for different cladding situations. In contrast, the overlap model needs sample preparation for each cladded coating.

For the sake of input details and further modification and perfection of the existing model it is recommended to continue with the overlap model and leave the laser parameter model for research where many samples are made with the same set-up, substrate and powder.

According to research [3] the grain size and information about their shape from transverse cuts alone are unsatisfactory in describing the microstructure formed during the laser cladding process. A more complete picture of the grain shape orientation should be offered by the observation of longitudinal cross-sections in the centre of the laser track.

The OIM software has excellent options to make elaborate analysis of samples. The interpretation should be done carefully, holding in mind what parts of the sample are being analysed. The overall preferential growth was as expected: towards the heat transfer perpendicular to the solidification front area.

As seen from the figures and plots, the displacement has a relation with the texture. The smaller the displacement during the cladding, the stronger the texture in the material. For more certainty about the dependence of the texture on the displacement, a systematic displacement sweep should be done.

4 Reference list

[1] E. Toyserkani, A. Khajepour, S.F. Corbin, *Laser cladding*, CRC press, 2014.

[2] J. Ion, *Laser processing of engineering materials: principles, procedure and industrial application*, Butterworth-Heineman, 2005.

[3] V. Ocelík, I. Furár, J.Th.M. De Hosson, *Microstructure and properties of laser clad coatings studied by orientation imaging microscopy,* Acta Materialia, 58, Elsevier, 2010.

[4] V. Ocelík, J. Th. M. De Hosson, *Thick metallic coatings produced by coaxial and side cladding: processing and properties,* Advances in Laser Materials Processing: Technology, Research and Application, Woodhead Publishing Limited, 427, 2010.

[5] A. Palavra, *Geometry and Microstructure of Laser Clad Coatings*, 2014.

[6] O. Nenadl, V. Ocelík, A. Palavra & J. Th. M. De Hosson, *Prediction of coating geometry: theory and experiment*, Surface and Contact Mechanics including Tribology XII, Vol. 91, WIT Press, 177-186, 2015.

[7] W.M. Kuipers, *Modelling the geometry of multi-layer laser cladded coatings*, 2015.

[8] V. Ocelík, O. Nenadl, A. Palavra, J.Th.M. De Hosson, *On the geometry of coating layers formed by overlap*, Surface & Coatings Technology, 242, Elsevier, 54-61, 2014.

[9] Y. Yingda, EM lab EBSD configuration, material science Norwegian University of Science & Technology, 2006.

[10] M. Nowell, *Cooking with EBSD - in-situ heating experiments*, Edax blog Elemental Analysis, 2014.

[11] S.A. David, S.S. Babu, and J.M. Vitek, *Welding: solidification and microstructure*, JOM: member journal of TMS, 2003.

[12] http://intecltd.co.kr/service/data/Add_file/3_PF-IPF_Eng.pdf

[13] H.E. Boyer, T.L. Gall, *Metals handbook*, Americal Society for Metals, Materials Park, OH, 1985.